New physics footprints in the angular distribution of $B_s \to D_s^*(\to D_s\gamma, D_s\pi)\tau\nu$ decays

Nilakshi Das[*] and Rupak Dutta[†]

National Institute of Technology Silchar, Silchar 788010, India

(Received 26 October 2021; accepted 7 March 2022; published 29 March 2022)

Hints of lepton flavor universality violation observed in various flavor ratios such as R_D, R_{D^*}, $R_{J/\psi}$, $P_\tau^{D^*}$, and $F_L^{D^*}$ in $B \to D^{(*)}\ell\nu$ and $B_c \to J/\psi\ell\nu$ charge current decays have opened new avenues to search for indirect evidences of beyond the standard model physics. Motivated by these anomalies, we perform a detailed angular analysis of $B_s \to D_s^*(\to D_s\gamma, D_s\pi)\ell\nu$ decays that proceed via similar $b \to c\ell\nu$ quark level transition. We use the most general effective Hamiltonian for $b \to cl\nu$ process and give predictions of several q^2 and $\cos\theta$ dependent observables for the $B_s \to D_s^*(\to D_s\gamma, D_s\pi)\ell\nu$ decays in the standard model and in the presence of various real and complex new physics couplings. The results pertaining to this decay are competent to address the anomalies in the charge current sector.

DOI: 10.1103/PhysRevD.105.055027

I. INTRODUCTION

Lepton flavor universality that treats the three generations of charged leptons (e, μ, τ) to be identical except the differences in their masses in the weak decays of flavor changing processes has exposed the possibility of new physics (NP) which lies beyond the Standard Model (SM). The hunt of new physics lies not just at the frontiers of the lepton flavor violating decays at the collider experiments but also in various other phenomena such as matter-antimatter asymmetry of the universe, dark matter, neutrino mass, mass hierarchy problem and so on. The B factories, since their inception, have been instrumental in exploring NP. In recent years, the B factories have reported several hints of lepton flavor universality violation in $b \to cl\nu$ charged current and $b \to sl^+l^-$ neutral current transition decays. More precisely, flavor sensitive observables such as R_D, R_{D^*}, $R_{J/\psi}$, $P_\tau^{D^*}$, and $F_L^{D^*}$ in $B \to D^{(*)}\ell\nu$ and $B_c \to J/\psi\ell\nu$ charge current decays deviate from the SM expectation at 1.4σ, 2.9σ, 1.8σ, 1.6σ, and 1.5σ level, respectively. Similarly, R_K, R_{K^*}, P_5' in $B \to K^{(*)}\ell^+\ell^-$ and $\mathcal{B}(B_s \to \phi\mu^+\mu^-)$ in neutral current decays deviate from the SM expectation at 3.1σ, 2.4σ, 3.3σ, and 3.6σ level, respectively. Although the results of several decay modes revealed the signature of lepton flavor universality violation, none of them are statistically significant to account for the evidence of new physics. The future upgrade of LHC with improved precision and with more number of new measurements can reduce the systematic error in the existing measurements and at the same time the efforts to study various similar decay modes eventually add up to tackle the possible new physics puzzle in semileptonic B decays. In the present context, we limit ourself to discuss the anomalies in the $b \to cl\nu$ charged current quark level transitions.

(i) Anomalies in R_D: The ratio of branching ratio R_D for the decay mode $B \to Dl\nu$ is defined as

$$R_D = \frac{\mathcal{B}(B \to D\tau\bar{\nu}_\tau)}{\mathcal{B}(B \to D\{e/\mu\}\bar{\nu}_{(e/\mu)})}. \tag{1}$$

A very precise SM prediction of $R_D = 0.299 \pm 0.003$ and $R_D = 0.300 \pm 0.008$ [1–6] was reported using the $B \to D$ form factors obtained in lattice QCD approach. In 2016, FLAG working group predicated the most accurate SM results of $R_D = 0.300 \pm 0.008$ by combining two lattice QCD results with the experimental form factor of $B \to Dl\nu$ obtained from *BABAR* [7] and BELLE [8]. In 2012, for the first time *BABAR* collaboration experimentally measured the value of the ratio of branching to be $R_D = 0.440 \pm 0.058 \pm 0.042$ [9]. This measurement was found to be deviated from the theoretical prediction at 2.6σ level. Later, BELLE collaboration in 2015 [10] measured the value to be $R_D = 0.375 \pm 0.064 \pm 0.026$. Similarly in the Moriond 2019, the BELLE collaboration announced the updated measurement in R_D and reported it to be $R_D = 0.307 \pm 0.037 \pm 0.016$ [11]. Although it is

[*]nilakshi_rs@phy.nits.ac.in
[†]rupak@phy.nits.ac.in

consistent with it's previous measurement, the average of all the three measurements obtained from the HFLAV still deviates at 1.4σ from the SM expectation [1–6]. Although the deviation from the SM prediction is decreased from 2.6σ to 1.4σ, the tension between theory and experiment still exists.

(ii) Anomalies in R_{D^*}: The ratio of branching ratio R_{D^*} for the decay mode $B \to D^* l\nu$ is defined as

$$R_{D^*} = \frac{\mathcal{B}(B \to D^* \tau \bar{\nu}_\tau)}{\mathcal{B}(B \to D^* \{e/\mu\} \bar{\nu}_{(e/\mu)})}. \tag{2}$$

The first SM prediction of $R_{D^*} = 0.252 \pm 0.003$ was reported in Ref. [12]. Several new calculations have become available since 2017 [5,6,13]. Although there are differences in the evaluation of the theoretical uncertainty, all the new calculations are found to be in very good agreement with each other. They are more robust and are consistent with the old predictions for R_{D^*} as well. The arithmetic average obtained by HFLAV is $R_{D^*} = 0.258 \pm 0.005$ [5,6,13]. As of $B \to D^*$ lattice QCD form factors are concerned, earlier some unquenched calculations at the zero recoil existed from the Fermilab Lattice and MILC Collaborations [14,15]. Very recently in 2021, using the lattice inputs, again the FNAL/MILC announced the first unquenched lattice calculation of $B \to D^*$ form factors [16] at nonzero recoil and reported the value of $R_{D^*} = 0.265 \pm 0.013$. First experimental measurement of $R_{D^*} = 0.332 \pm 0.024 \pm 0.018$ was reported by *BABAR* collaboration [17] and it was found to be deviated at 2.7σ from the SM predication. Later in 2015, 2016, and 2017, Belle collaboration measured the value of R_{D^*} to be $0.293 \pm 0.038 \pm 0.015$ [10], $0.302 \pm 0.030 \pm 0.011$ [18] and $0.270 \pm 0.035^{+0.028}_{-0.025}$ [19], respectively. Similarly, in the year 2015 and 2017, LHCb collaboration also measured the value of R_{D^*} to be $0.336 \pm 0.027 \pm 0.030$ [20] and $0.291 \pm 0.019 \pm 0.029$ [21], respectively. The recent update of R_{D^*} measurement from the Belle collaboration [22] announced in the Moriond 2019 is $R_{D^*} = 0.283 \pm 0.018 \pm 0.014$. At present, the average of various measurements of R_{D^*} from HFLAV still deviates from the SM expectation at the level of 2.9σ.

(iii) Anomalies in $R_{J/\psi}$: The ratio of branching ratio $R_{J/\psi}$ for the decay mode $B_c \to J/\psi l\nu$ is defined as

$$R_{J/\psi} = \frac{\mathcal{B}(B_c \to J/\psi \tau \bar{\nu}_\tau)}{\mathcal{B}(B_c \to J/\psi \{e/\mu\} \bar{\nu}_{(e/\mu)})}. \tag{3}$$

The SM prediction of $R_{J/\psi}$ can be found in the Refs. [23–29]. In addition, the authors in Ref. [30] provide the SM bound to be $R_{J/\psi} \in [0.20, 0.39]$ at 95% confidence level. Very recently, the HPQCD collaboration reported the first lattice QCD results of $R_{J/\psi}$ and reported it to be 0.2582 ± 0.0038 [31]. The experimental measurement of $R_{J/\psi}$ from the LHCb collaboration in 2017 has reported the value of $R_{J/\psi} = 0.71 \pm 0.17 \pm 0.18$. This measurement of $R_{J/\psi}$ deviates from the SM prediction at 1.8σ level.

(iv) Anomalies in $P_\tau^{D^*}$ and $F_L^{D^*}$: The τ polarization fraction and the longitudinal polarization fraction of D^* meson in $B \to D^* \tau\nu$ decays are defined as

$$P_\tau^{D^*} = \frac{\Gamma^+(B \to D^* \tau \bar{\nu}_\tau) - \Gamma^-(B \to D^* \tau \bar{\nu}_\tau)}{\Gamma(B \to D^* \tau \bar{\nu}_\tau)},$$
$$F_L^{D^*} = \frac{\Gamma(B \to D_L^* \tau \bar{\nu}_\tau)}{\Gamma(B \to D^* \tau \bar{\nu}_\tau)}. \tag{4}$$

The measured value of the τ polarization fraction $P_\tau^{D^*} = -0.38 \pm 0.51^{+0.21}_{-0.16}$ [32,33] deviates from the SM prediction of 0.497 ± 0.013 [34] at 1.6σ level. Similarly, for $F_L^{D^*}$, the measured value $F_L^{D^*} = 0.60 \pm 0.08 \pm 0.035$ [35] deviates from the SM expectation of 0.46 ± 0.04 [36] at 1.5σ level.

So far till date there have been several model independent and model dependent NP analysis on $b \to c l\nu$ decays. We report here an incomplete list of various literatures [37–81]. Recently, in Refs. [82,83], the authors calculate the best fit values of vector, scalar, and tensor NP couplings in $1D$ and $2D$ scenarios by fitting the experimental measurements of $R_{D^{(*)}}$, $P_\tau^{D_s^*}$, and F_L by considering the correlation between the observable $R_D - R_{D^*}$. Similarly, in Ref. [61], the authors obtained the best fit values of NP Wilson coefficients (WC) by considering the experimental values of $R_D - R_{D^*}$ in a Bayesian statistical approach assuming complex NP WCs. Moreover, in Ref [84], the authors perform a global fit of NP WCs by considering the constraints coming from the measured value of $R_{D^{(*)}}$, $P_\tau^{D^*}$, $F_L^{D^*}$, differential q^2 distribution of $B \to D\tau\nu$ and $B \to D^*\tau\nu$ decays and branching fraction of $B_c \to \tau\bar{\nu}_\tau$ decays.

The SM analysis of $B_s \to D_s^* l\nu$ decays has been performed by several authors using the form factors obtained in the constituent quark meson (CQM) model [85], the QCD sum rule [86,87], the light cone sum rule (LCSR) [88,89], the covariant light-front quark model (CLFQM) [90], the instantaneous Bethe-Salpeter equation [91,92], the lattice QCD at zero recoil point [93], the perturbative QCD approach [94,95], the BGL parametrization of lattice QCD data. [96] and the relativistic quark model (RQM) based on the quasipotential approach [97]. In Ref. [98], the authors perform a model independent analysis of NP effects in $B_s \to D_s^* l\nu$ decays by using the RQM form factors of Ref. [97]. They, however, treat D_s^* meson to be stable and did not consider any further decay of D_s^* to $D_s\gamma$ or $D_s\pi$.

In the present paper, we use the most general effective Lagrangian in the presence of NP and perform a detail angular analysis of $B_s \to D_s^*(\to D_s\gamma, D_s\pi) l\nu$ decays using the lattice QCD form factor results in the full q^2 range. Among the two decay channels, the probability of D_s^* going to $D_s\gamma$ is 93%, whereas, for $D_s^* \to D_s\pi$, it is 5%. In this analysis we treat the NP WCs to be both real and complex. We give prediction of the branching fraction, longitudinal polarization fraction of D_s^* meson, forward backward asymmetry and several other angular observables pertinent to $B_s \to D_s^*(\to D_s\gamma, D_s\pi)l\nu$ decays.

Study of this decay channel is well motivated for several reasons. From the experimental point of view, very recently, LHCb collaboration has provided a complementary information regarding the CKM matrix element V_{cb} using this decay channel. Similarly, LHCb collaboration has also reported the measured shape of the normalized differential decay distribution with respect to q^2. It will allow to make a direct comparison between the experimental measurements with its theoretical values. Moreover, BELLE collaboration is accumulating large data samples which will help in measuring the branching fractions to a very good precision. A total of $(6.53 \pm 0.66) \times 10^6$ $B_s\bar{B}_s$ pair is obtained at the BELLE detector [99] at electron-positron collider KEKB asymmetric energy. In BELLE-II the statistics will be increased by a factor of 40, and in the next decade the datas are expected to be more than 50 times. Hence a precise measurement of observables pertaining to $B_s \to D_s^* l\nu$ decays may be feasible in near future which eventually will be crucial to reveal the evidence of lepton flavor universality violation in B meson decays. At the same time, from theoretical point of view, very recently in 2021, first lattice QCD results for $B_s \to D_s^*$ form factors have been reported by the HPQCD collaboration [100]. From the lattice QCD point of view, the $B_s \to D_s^*$ form factors have an advantage over the $B \to D^*$ form factors mainly for two reasons. First, the $B_s \to D_s^*$ does not contain the valance u/d quarks. Second, the D_s^* meson can be treated as stable as there is no Zweing-allowed strong two body decays because of its very narrow width.

This paper is organized as follows. In Sec. II, we start with the most general effective weak Lagrangian for $b \to cl\nu$ decays in the presence of vector, scalar and tensor NP operators. We also report the relevant formula for all the observables pertaining to $B_s \to D_s^*(\to D_s\gamma, D_s\pi)l\nu$ decays in Sec. II. In Sec. III, we discuss the results obtained in the SM and in the presence of several NP couplings. Finally, we conclude with a brief summary of our results in Sec. IV.

II. THEORETICAL FRAMEWORK

In the presence of NP, the effective weak Lagrangian for the $b \to cl\nu$ transition decays at renormalization scale $\mu = m_b$ can be written as [101,102]

$$\begin{aligned}\mathcal{L}_{\rm eff} = -\frac{4G_F}{\sqrt{2}} V_{cb}\{&(1+g_{V_L})\bar{l}_L\gamma_\mu\nu_L\bar{c}_L\gamma^\mu b_L + g_{V_R}\bar{l}_L\gamma_\mu\nu_L\bar{c}_R\gamma^\mu b_R \\ &+ g_{S_L}\bar{l}_R\nu_L\bar{c}_R b_L + g_{S_R}\bar{l}_R\nu_L\bar{c}_L b_R + g_{T_L}\bar{l}_R\sigma_{\mu\nu}\nu_L\bar{c}_R\sigma^{\mu\nu}b_L\} + \text{H.c.},\end{aligned} \tag{5}$$

where, G_F is the Fermi coupling constant and V_{cb} is the Cabibbo-Kobayashi-Maskawa (CKM) matrix element. The vector, scalar, and tensor type NP interactions denoted by $g_{V_{L,R}}$, $g_{S_{L,R}}$, and g_{T_L} NP couplings are associated with left handed neutrinos. We have not considered the right handed neutrino interactions in our analysis.

A. Angular decay distribution of $B_s \to D_s^*(\to D_s\gamma)l\nu$ decay mode

The four body differential decay distribution for the $B_s \to D_s^*(\to D_s\gamma)l\nu$ decay can be expressed in terms of the angular coefficients as [103]

$$\begin{aligned}\frac{d^4\Gamma(B \to D_s^*(\to D_s\gamma)l\nu)}{dq^2 d\cos\theta_l d\cos\theta_{D_s} d\phi} = \mathcal{N}_\gamma P_{D_s*}\left(1-\frac{m_l^2}{q^2}\right)^2 &\{I_{1s}\sin^2\theta_{D_s} + I_{1c}(3+\cos 2\theta_{D_s}) + (I_{2s}\sin^2\theta_{D_s} + I_{2c}(3+\cos 2\theta_{D_s})) \\ &\times \cos 2\theta_l + I_3 \sin^2\theta_{D_s}\sin^2\theta_l\cos 2\phi + I_4\sin 2\theta_{D_s}\sin 2\theta_l\cos\phi + I_5\sin 2\theta_{D_s}\sin\theta_l\cos\phi \\ &+ (I_{6s}\sin^2\theta_{D_s} + I_{6c}(3+\cos 2\theta_{D_s}))\cos\theta_l + I_7\sin 2\theta_{D_s}\sin\theta_l\sin\phi \\ &+ I_8\sin 2\theta_{D_s}\sin 2\theta_l\sin\phi + I_9\sin^2\theta_{D_s}\sin^2\theta_l\sin 2\phi\}\end{aligned} \tag{6}$$

where the three momentum vector of the D_s^* meson and the normalization constant are defined as

$$|P_{D_s^*}| = \sqrt{\lambda(m_{B_s}^2, m_{D_s^*}^2, q^2)}/2m_{B_s}, \qquad N_\gamma = \frac{3G_F^2|V_{cb}|^2\mathcal{B}(D_s^* \to D_s\gamma)}{128(2\pi)^4 m_{B_s^2}}. \tag{7}$$

In the presence of vector, scalar and tensor NP couplings, the angular coefficients I_i, where $i = 1, \ldots 6$, can be expressed as [103]

$$I_i = |1+\epsilon_V|^2 I_i^{\rm SM} + |\epsilon_R|^2 I_i^{NP,R} + |\epsilon_P|^2 I_i^{NP,T} + 2{\rm Re}[\epsilon_R(1+\epsilon_V^*)] I_i^{INT,R} + 2{\rm Re}[\epsilon_P(1+\epsilon_V^*)] I_i^{INT,P}$$
$$+ 2{\rm Re}[\epsilon_T(1+\epsilon_V^*)] I_i^{INT,T} + 2{\rm Re}[\epsilon_R\epsilon_T^*] I_i^{INT,RT} + 2{\rm Re}[\epsilon_P\epsilon_T^*] I_i^{INT,PT} + 2{\rm Re}[\epsilon_P\epsilon_R^*] I_i^{INT,PR}. \quad (8)$$

Similarly, the angular coefficients I_7, I_8, and I_9 can be written as

$$\begin{aligned} I_7 &= 2{\rm Im}[\epsilon_R(1+\epsilon_V^*)] I_7^{INT,R} + 2{\rm Im}[\epsilon_P(1+\epsilon_V^*)] I_7^{INT,P} + 2{\rm Im}[\epsilon_T(1+\epsilon_V^*)] I_7^{INT,T} \\ &\quad + 2{\rm Im}[\epsilon_R\epsilon_T^*] I_7^{INT,RT} + 2{\rm Im}[\epsilon_P\epsilon_T^*] I_7^{INT,PT} + 2{\rm Im}[\epsilon_P\epsilon_R^*] I_7^{INT,RT}, \\ I_{(8/9)} &= 2{\rm Im}[\epsilon_R(1+\epsilon_V^*)] I_{(8/9)}^{INT,R}, \end{aligned} \quad (9)$$

where

$$\epsilon_V = g_{V_L}, \qquad \epsilon_R = g_{V_R}, \qquad \epsilon_P = g_{S_R} - g_{S_L} \qquad \epsilon_S = g_{S_R} + g_{S_L} \qquad \epsilon_T = g_{T_L}. \quad (10)$$

Here $I_i^{\rm SM}$ represents the angular coefficients in the SM and all other terms correspond to NP, interference of NP with NP, and interference of SM with NP, respectively. We refer to Ref. [103] for all the omitted details.

1. The q^2 dependent observables

We define several q^2 dependent observables for the $B_s \to D_s^*(\to D_s\gamma)l\nu$ decay mode.

(i) The differential branching ratio, the lepton forward-backward asymmetry $A_{FB}^l(q^2)$, the forward-backward asymmetry of transversely polarized D_s^* meson $A_{FB}^T(q^2)$, the longitudinal polarization fraction of the D_s^* meson $F_L(q^2)$ and the convexity parameter $C_F^l(q^2)$ are defined as [61]

$$\begin{aligned} &\frac{d\Gamma}{dq^2}(q^2) = \mathcal{N}_\gamma |\vec{P}_{D_s^*}| \left(1-\frac{m_l^2}{q^2}\right)^2 \frac{16}{9}\pi(3I_{1s}+12I_{1c}-I_{2s}-4I_{2c}) \\ &A_{FB}^l(q^2) = \frac{8\pi}{3}\frac{\mathcal{N}_\gamma |\vec{P}_{D_s^*}|(1-\frac{m_l^2}{q^2})^2(I_{6s}+4I_{6c})}{d\Gamma/dq^2}, \qquad A_{FB}^T(q^2) = \frac{32\pi}{3}\frac{\mathcal{N}_\gamma |\vec{P}_{D_s^*}|(1-\frac{m_l^2}{q^2})^2 I_{6c}}{d\Gamma_T/dq^2}, \\ &F_L(q^2) = \frac{16\pi}{9}\frac{\mathcal{N}_\gamma |\vec{P}_{D_s^*}|(1-\frac{m_l^2}{q^2})^2(3I_{1s}-I_{2s})}{d\Gamma/dq^2}, \qquad C_F^l(q^2) = \frac{32\pi}{3}\frac{\mathcal{N}_\gamma |\vec{P}_{D_s^*}|(1-\frac{m_l^2}{q^2})^2(I_{2s}+4I_{2c})}{d\Gamma/dq^2}. \end{aligned} \quad (11)$$

where

$$\frac{d\Gamma_T}{dq^2} = \frac{16\pi}{9}\mathcal{N}_\gamma |\vec{P}_{D_s^*}| \left(1-\frac{m_l^2}{q^2}\right)^2 (12I_{1c}-4I_{2c}).$$

(ii) The angular observables $A_3(q^2)$, $A_4(q^2)$, $A_5(q^2)$, $A_{6s}(q^2)$, $A_7(q^2)$, $A_8(q^2)$, and $A_9(q^2)$ are defined as [61]

$$\begin{aligned} &A_3(q^2) = \frac{16}{9}\frac{\mathcal{N}_\gamma |\vec{P}_{D_s^*}|(1-\frac{m_l^2}{q^2})^2 I_3}{d\Gamma/dq^2}, \qquad A_4(q^2) = -\frac{64}{9}\frac{\mathcal{N}_\gamma |\vec{P}_{D_s^*}|(1-\frac{m_l^2}{q^2})^2 I_4}{d\Gamma/dq^2}, \\ &A_5(q^2) = -\frac{8\pi}{3}\frac{\mathcal{N}_\gamma |\vec{P}_{D_s^*}|(1-\frac{m_l^2}{q^2})^2 I_5}{d\Gamma/dq^2}, \qquad A_{6s}(q^2) = -\frac{288\pi}{24}\frac{\mathcal{N}_\gamma |\vec{P}_{D_s^*}|(1-\frac{m_l^2}{q^2})^2 I_{6s}}{d\Gamma/dq^2}, \\ &A_7(q^2) = -\frac{8\pi}{3}\frac{\mathcal{N}_\gamma |\vec{P}_{D_s^*}|(1-\frac{m_l^2}{q^2})^2 I_7}{d\Gamma/dq^2}, \qquad A_8(q^2) = \frac{64}{9}\frac{\mathcal{N}_\gamma |\vec{P}_{D_s^*}|(1-\frac{m_l^2}{q^2})^2 I_8}{d\Gamma/dq^2}, \\ &A_9(q^2) = \frac{16}{9}\frac{\mathcal{N}_\gamma |\vec{P}_{D_s^*}|(1-\frac{m_l^2}{q^2})^2 I_9}{d\Gamma/dq^2}. \end{aligned} \quad (12)$$

(iii) The ratio of branching fraction is defined as follows

$$R_{D_s^*}(q^2) = \frac{d\Gamma/dq^2|_{\tau-\text{mode}}}{d\Gamma/dq^2|_{e-\text{mode}}}. \tag{13}$$

2. The $\cos\theta$ dependent observables

We also define several $\cos\theta_{D_s}$ and $\cos\theta_l$ dependent observables. They are

$$\begin{aligned}
F_L(\cos\theta_{D_s}) &= \frac{\mathcal{N}_\gamma|\vec{P}_{D_s^*}|(1-\frac{m_l^2}{q^2})^2 2\pi\int_{q^2_{\min}}^{q^2_{\max}}(2I_{1s}-\frac{2}{3}I_{2s})(1-\cos^2\theta_{D_s})dq^2}{\Gamma(B_s\to D_s^*(\to D\gamma)l\nu)}\\
F_T(\cos\theta_{D_s}) &= \frac{\mathcal{N}_\gamma|\vec{P}_{D_s^*}|(1-\frac{m_l^2}{q^2})^2 4\pi\int_{q^2_{\min}}^{q^2_{\max}}(2I_{1c}-\frac{2}{3}I_{2c})(1+\cos^2\theta_{D_s})dq^2}{\Gamma(B_s\to D_s^*(\to D\gamma)l\nu)}\\
F_L(\cos\theta_l) &= \frac{8\pi}{3}\frac{\mathcal{N}_\gamma|\vec{P}_{D_s^*}|(1-\frac{m_l^2}{q^2})^2\int_{q^2_{\min}}^{q^2_{\max}}(I_{1s}+I_{2s}(2\cos^2\theta_l-1)+I_{6s}\cos\theta_l)dq^2}{\Gamma(B_s\to D_s^*(\to D_s\gamma)l\nu)}\\
F_T(\cos\theta_l) &= \frac{32\pi}{3}\frac{\mathcal{N}_\gamma|\vec{P}_{D_s^*}|(1-\frac{m_l^2}{q^2})^2\int_{q^2_{\min}}^{q^2_{\max}}(I_{1c}+I_{2c}(2\cos^2\theta_l-1)+I_{6c}\cos\theta_l)dq^2}{\Gamma(B_s\to D_s^*(\to D_s\gamma)l\nu)}\\
A_{FB}^l(\cos\theta_{D_s}) &= \frac{\mathcal{N}_\gamma|\vec{P}_{D_s^*}|(1-\frac{m_l^2}{q^2})^2 2\pi\int_{q^2_{\min}}^{q^2_{\max}}[(I_{6s}+2I_{6c})+(2I_{6c}-I_{6s})\cos^2\theta_{D_s}]dq^2}{d\Gamma/d\cos\theta_{D_s}},
\end{aligned} \tag{14}$$

where

$$\frac{d\Gamma}{d\cos\theta_{D_s}} = \frac{4\pi}{3}\int_{q^2_{\min}}^{q^2_{\max}}\mathcal{N}_\gamma|\vec{P}_{D_s^*}|\left(1-\frac{m_l^2}{q^2}\right)^2[(3I_{1s}-I_{2s}+6I_{1c}-2I_{2c})+(I_{2s}-3I_{1s}+6I_{1c}-2I_{2c})\cos^2\theta_{D_s}]dq^2.$$

B. Angular decay distribution of $B_s\to D_s^*(\to D_s\pi)l\nu$ decay mode

Starting with the effective Lagrangian of Eq. (5), the four body differential decay distribution of $B_s\to D_s^*(\to D_s\pi)l\nu$ can be written as follows [61,104].

$$\begin{aligned}
\frac{d^4\Gamma(B\to D_s^*(\to D_s\pi)l\nu)}{dq^2 d\cos\theta_l d\cos\theta_{D_s}d\phi} = \frac{9}{32\pi}\{&I_{1s}\sin^2\theta_{D_s}+I_{1c}\cos^2\theta_{D_s}+(I_{2s}\sin^2\theta_{D_s}+I_{2c}\cos^2\theta_{D_s})\cos 2\theta_l\\
&+(I_3\cos 2\phi+I_9\sin 2\phi)\sin^2\theta_{D_s}\sin^2\theta_l+(I_4\cos\phi+I_8\sin\phi)\sin 2\theta_{D_s}\sin 2\theta_l\\
&+(I_5\cos\phi+I_7\sin\phi)\sin 2\theta_{D_s}\sin\theta_l+(I_{6s}\sin^2\theta_{D_s}+I_{6c}\cos^2\theta_{D_s})\cos\theta_l\},
\end{aligned} \tag{15}$$

where the angular coefficients are [61,104]

$$\begin{aligned}
I_{1c} &= N_F\left[2\left(1+\frac{m_l^2}{q^2}\right)(\mathcal{A}_0^L+4|\mathcal{A}_{T0}^L|^2)-\frac{16m_l}{\sqrt{q^2}}\mathrm{Re}[\mathcal{A}_0^L\mathcal{A}_{T0}^{L*}]+\frac{4m_l^2}{q^2}|\mathcal{A}_{tP}^L|^2\right]\\
I_{1s} &= N_F\left[\frac{1}{2}\left(3+\frac{m_l^2}{q^2}\right)(|\mathcal{A}_\perp^L|^2+|\mathcal{A}_{||}^L|^2)+2\left(1+\frac{3m_l^2}{q^2}\right)(|\mathcal{A}_{T\perp}^L|^2+|\mathcal{A}_{T||}^L|^2)-8\frac{m_l}{\sqrt{q^2}}\mathrm{Re}[\mathcal{A}_\perp^L\mathcal{A}_{T\perp}^{L*}+\mathcal{A}_{||}^L\mathcal{A}_{T||}^{L*}]\right.\\
I_{2c} &= -2N_F\left(1-\frac{m_l^2}{q^2}\right)(|\mathcal{A}_0^L|^2-|\mathcal{A}_{T0}^L|^2)\\
I_{2s} &= \frac{1}{2}N_F\left(1-\frac{m_l^2}{q^2}\right)(|\mathcal{A}_\perp^L|^2+|\mathcal{A}_{||}^L|^2)-4(|\mathcal{A}_{T\perp}^L|^2+|\mathcal{A}_{T||}^L|^2)\\
I_3 &= N_F\left(1-\frac{m_l^2}{q^2}\right)(|\mathcal{A}_\perp^L|^2-|\mathcal{A}_{||}^L|^2-4(|\mathcal{A}_{T\perp}^L|^2+|\mathcal{A}_{T||}^L|^2))
\end{aligned}$$

$$
\begin{aligned}
I_4 &= \sqrt{2}N_F\left(1-\frac{m_l^2}{q^2}\right)\mathrm{Re}[\mathcal{A}_0^L\mathcal{A}_{||}^{L*}-4\mathcal{A}_{T0}^L\mathcal{A}_{T||}^{L*}] \\
I_5 &= 2\sqrt{2}N_F\left[\mathrm{Re}\left[\left(\mathcal{A}_0^L-2\frac{m_l}{\sqrt{q^2}}\mathcal{A}_{T0}^L\right)\left(\mathcal{A}_\perp^{L*}-2\frac{m_l}{\sqrt{q^2}}\mathcal{A}_{T\perp}^{L*}\right)\right]-\frac{m_l^2}{q^2}\mathrm{Re}\left[\mathcal{A}_{tP}^{L*}\left(\mathcal{A}_{||}^L-2\frac{m_l}{\sqrt{q^2}}\mathcal{A}_{T||}^L\right)\right]\right. \\
I_{6c} &= N_F\frac{8m_l^2}{q^2}\mathrm{Re}\left[\mathcal{A}_{tP}^{L*}\left(\mathcal{A}_0^L-2\frac{\sqrt{q^2}}{m_l}\mathcal{A}_{T0}^L\right)\right] \\
I_{6s} &= 4N_F\mathrm{Re}\left[\left(\mathcal{A}_{||}^L-2\frac{m_l}{\sqrt{q^2}}\mathcal{A}_{T||}^L\right)\left(\mathcal{A}_\perp^{L*}-2\frac{m_l}{\sqrt{q^2}}\mathcal{A}_{T\perp}^{L*}\right)\right] \\
I_7 &= -2\sqrt{2}N_F\left[\mathrm{Im}\left[\left(\mathcal{A}_0^L-2\frac{m_l}{q^2}\mathcal{A}_{T0}^L\right)\left(\mathcal{A}_{||}^{L*}-2\frac{m_l}{q^2}\mathcal{A}_{T||}^{L*}\right)+\frac{m_l^2}{q^2}\mathrm{Im}\left[\mathcal{A}_{tP}^{L*}\left(\mathcal{A}_\perp^L-2\frac{q^2}{m_l}\mathcal{A}_{T\perp}^L\right)\right]\right]\right. \\
I_8 &= \sqrt{2}N_F\left(1-\frac{m_l^2}{q^2}\right)\mathrm{Im}[\mathcal{A}_0^{L*}\mathcal{A}_\perp^L-4\mathcal{A}_{T0}^{L*}\mathcal{A}_{T\perp}^L] \\
I_9 &= 2N_F\left(1-\frac{m_l^2}{q^2}\right)\mathrm{Im}[\mathcal{A}_{||}^L\mathcal{A}_\perp^{L*}-4\mathcal{A}_{T||}^L\mathcal{A}_{T\perp}^{L*}],
\end{aligned}
\tag{16}
$$

with

$$
N_F = \frac{G_F^2|V_{cb}|^2}{2^7 3\pi^3 m_{B_s}^3}q^2\lambda_{D_s^*}^{1/2}\left(1-\frac{m_l^2}{q^2}\right)^2\mathcal{B}(D_s^*\to D_s\pi). \tag{17}
$$

The longitudinal, transverse, and timelike component of amplitude $A^L_{T0,T\perp,T||}$, written in terms of NP couplings, are taken from Ref. [104]. We refer to Ref. [104] for the omitted details.

1. The q^2 dependent observables

(i) The differential branching ratio, the lepton forward-backward asymmetry $A^l_{FB}(q^2)$, the forward-backward asymmetry of transversely polarized D_s^* meson $A^T_{FB}(q^2)$, the longitudinal polarization fraction of the D_s^* meson $F_L(q^2)$ and the convexity parameter $C^l_F(q^2)$ can be defined as [61]

$$
\begin{aligned}
&\frac{d\Gamma}{dq^2}(q^2)=\frac{1}{4}(6I_{1s}+3I_{1c}-2I_{2s}-I_{2c}), \qquad A^l_{FB}(q^2)=\frac{3}{8}\frac{(I_{6c}+2I_{6s})}{d\Gamma/dq^2}, \\
&F_L(q^2)=\frac{1}{4}\frac{(3I_{1c}-I_{2c})}{d\Gamma/dq^2} \qquad A^T_{FB}(q^2)=\frac{6}{8}\frac{I_{6s}}{d\Gamma_T/dq^2}, \qquad C^l_F(q^2)=\frac{6}{8}\frac{(2I_{2c}+4I_{2s})}{d\Gamma/dq^2}.
\end{aligned}
\tag{18}
$$

where

$$
\frac{d\Gamma_T}{dq^2}=\frac{1}{4}(6I_{1s}-2I_{2s}). \tag{19}
$$

(ii) The angular observables $A_3(q^2)$, $A_4(q^2)$, $A_5(q^2)$, $A_{6s}(q^2)$, $A_7(q^2)$, $A_8(q^2)$, and $A_9(q^2)$ can be defined as [61]

$$
\begin{aligned}
A_3(q^2)&=\frac{1}{2\pi}\frac{I_3}{d\Gamma/dq^2} \qquad A_4(q^2)=-\frac{2}{\pi}\frac{I_4}{d\Gamma/dq^2} \\
A_5(q^2)&=-\frac{3}{4}\frac{I_5}{d\Gamma/dq^2} \qquad A_{6s}(q^2)=-\frac{27}{8}\frac{I_{6s}}{d\Gamma/dq^2} \\
A_7(q^2)&=-\frac{3}{4}\frac{I_7}{d\Gamma/dq^2} \qquad A_8(q^2)=\frac{2}{\pi}\frac{I_8}{d\Gamma/dq^2} \\
A_9(q^2)&=\frac{1}{2\pi}\frac{I_9}{d\Gamma/dq^2}.
\end{aligned}
\tag{20}
$$

2. The $\cos\theta$ dependent observables

The $\cos\theta_{D_s}$ and $\cos\theta_l$ dependent observables can be defined as follows [64].

$$
\begin{aligned}
F_L(\cos\theta_{D_s}) &= \frac{9}{16}\frac{\int_{q^2_{\min}}^{q^2_{\max}}(2I_{1c}-\frac{2}{3}I_{2c})\cos^2\theta_{D_s}dq^2}{\Gamma(B_s\to D_s^*(\to D_s\pi)l\nu)}\\
F_T(\cos\theta_{D_s}) &= \frac{9}{16}\frac{\int_{q^2_{\min}}^{q^2_{\max}}(2I_{1s}-\frac{2}{3}I_{2s})(1-\cos^2\theta_{D_s})dq^2}{\Gamma(B_s\to D_s^*(\to D_s\pi)l\nu)}\\
F_L(\cos\theta_l) &= \frac{9}{24}\frac{\int_{q^2_{\min}}^{q^2_{\max}}(I_{1c}+I_{2c}(2\cos^2\theta_l-1)+I_{6c}\cos\theta_l)dq^2}{\Gamma(B_s\to D_s^*(\to D_s\pi)l\nu)}\\
F_T(\cos\theta_l) &= \frac{9}{12}\frac{\int_{q^2_{\min}}^{q^2_{\max}}(I_{1s}+I_{2s}(2\cos^2\theta_l-1)+I_{6s}\cos\theta_l)dq^2}{\Gamma(B_s\to D_s^*(\to D_s\pi)l\nu)}\\
A^l_{FB}(\cos\theta_{D_s}) &= \frac{9}{16}\frac{\int_{q^2_{\min}}^{q^2_{\max}}(I_{6s}+(I_{6c}-I_{6s})\cos^2\theta_{D_s})dq^2}{d\Gamma/d\cos\theta_{D_s}},
\end{aligned}
\tag{21}
$$

where

$$
\frac{d\Gamma}{d\cos\theta_{D_s}} = \frac{9}{24}\int_{q^2_{\min}}^{q^2_{\max}}[(3I_{1s}-I_{2s})+(I_{2s}-3I_{1s}+3I_{1c}-2I_{2c})\cos^2\theta_{D_s}]dq^2. \tag{22}
$$

In general, for all q^2, the coefficients in $D\pi$ and $D\gamma$ angular distributions obey the following relations.

$$
\frac{I^\pi_{1s}}{4I^\gamma_{1c}} = \frac{I^\pi_{1c}}{2I^\gamma_{1s}} = \frac{I^\pi_{2s}}{4I^\gamma_{2c}} = \frac{I^\pi_{2c}}{2I^\gamma_{2s}} = \frac{I^\pi_{6s}}{4I^\gamma_{6c}} = \frac{I^\pi_{6c}}{2I^\gamma_{6s}} = -\frac{I^\pi_{3}}{2I^\gamma_{3}} = -\frac{I^\pi_{4}}{2I^\gamma_{4}} = -\frac{I^\pi_{5}}{2I^\gamma_{5}} = 1.
$$

Using these relations one can easily see that the observables $R_{D_s^*}(q^2)$, $A^l_{FB}(q^2)$, $A^T_{FB}(q^2)$, $F_L(q^2)$, $C^l_F(q^2)$, $F_L(\cos\theta_l)$ and $F_T(\cos\theta_l)$ are numerically equal in both $D_s\pi$ and $D_s\gamma$ decay channels.

III. RESULTS AND DISCUSSION

A. Input parameters

In Table I, we report all the theory inputs such as the masses of various mesons, leptons, the branching fraction of $\mathcal{B}(D_s^*\to D_s\gamma)$, $\mathcal{B}(D_s^*\to D_s\pi)$ and mass of b quark and c quark evaluated at renormalization scale $\mu = m_b$ [105]. The mass parameters are expressed in GeV unit and the B_s meson life time τ_{B_s} is expressed in second. We consider the uncertainties associated with the CKM matrix element $|V_{cb}|$ and the relevant vector and axial vector form factor inputs V, A_0, A_1 and A_2 of Ref. [100]. The relevant formula for the form factors pertinent for our discussion, taken from Ref. [100], is

$$
F(q^2) = \frac{1}{P(q^2)}\sum_{n=0}^{3}a_n z^n(q^2,t_0), \tag{23}
$$

where F stands for the form factors V, A_0, A_1, A_2 and a_0, a_1, a_2, a_3 are the z-expansion coefficients. The pole function $P(q^2)$ and $z(q^2,t_0)$ are defined as

TABLE I. Theory input parameters.

Parameters	Values	Parameters	Values	Parameters	Values
m_{B_s}	5.36677	$m_{D_s^*}$	2.112	m_e	$0.5109989461\times10^{-3}$
m_b	4.18	m_c	0.91	$\lvert V_{cb}\rvert$	0.0409(11)
m_B	5.27964	m_{D^*}	2.010	m_τ	1.77682
$\mathcal{B}(D_s^*\to D_s\pi)$	5.8×10^{-2}	$\mathcal{B}(D_s^*\to D_s\gamma)$	93.5×10^{-2}		
G_F	1.1663787×10^{-5}	τ_{B_s}	1.515×10^{-12}		

TABLE II. Form factor input parameters.

	a_0	a_1	a_2	a_3	M_{pole}			
A_0	0.1046(79)	−0.39(15)	0.02(98)	−0.03(1.00)	6.275	6.872	7.25	
A_1	0.0536(28)	0.020(75)	0.09(81)	0.10(99)	6.745	6.75	7.15	7.15
A_2	0.051(15)	0.02(26)	−0.35(79)	−0.07(99)	6.745	6.75	7.15	7.15
V	0.102(14)	−0.27(30)	−0.007(0.998)	−3e − 05 + −1	6.335	6.926	7.02	7.28

$$P(q^2) = \prod_{M_{\text{pole}}} z(q^2, M^2_{\text{pole}}) \quad z(q^2, t_0) = \frac{\sqrt{t_+ - q^2} - \sqrt{t_+ - t_0}}{\sqrt{t_+ - q^2} + \sqrt{t_+ - t_0}}. \tag{24}$$

where, $t_0 = (M_{B_s} - M_{D_s^*})^2$, $t_+ = (M_B + M_{D^*})^2$ and the pole masses are represented by M_{pole}. In Table II, we report the form factor inputs relevant for our analysis. The uncertainty associated with these parameters are written within parenthesis.

We have used the equation of motion to find out the relevant tensor form factors so that

$$T_1(q^2) = \frac{m_b + m_c}{m_{B_s} + m_{D_s^*}} V(q^2), \quad T_2(q^2) = \frac{m_b - m_c}{m_{B_s} - m_{D_s^*}} A_1(q^2),$$
$$T_3(q^2) = -\frac{m_b - m_c}{q^2} [m_{B_s}(A_1(q^2) - A_2(q^2)) + m_{D_s^*}(A_2(q^2) + A_1(q^2) - 2A_0(q^2))]. \tag{25}$$

B. SM prediction

We report the SM central value and the 1σ uncertainty associated with several observables such as the branching ratio (BR), the ratio of branching ratio ($R_{D_s^*}$), the forward backward asymmetry (A^l_{FB}), the convexity parameter (C^l_F), the forward backward asymmetry for the transversely polarized D_s^* meson (A^T_{FB}), the longitudinal polarization fraction of D_s^* meson (F_L), the angular observables such as A_3, A_4, A_5, A_{6s}, A_7, A_8, and A_9 for both e and τ mode in Table III. Our observations are as follows.

(i) The branching ratio of $B_s \to D_s^*(\to D_s\pi)l\nu$ mode is found to be of $\mathcal{O}(10^{-3})$, whereas the branching ratio of $B_s \to D_s^*(\to D_s\gamma)l\nu$ decay mode is obtained to be of $\mathcal{O}(10^{-2})$.

(ii) As expected, the central value and the 1σ uncertainty associated with $R_{D_s^*}$, A^l_{FB}, C^l_F, A^T_{FB}, and F_L is exactly same for the $B_s \to D_s^*(\to D_s\gamma)l\nu$ and the $B_s \to D_s^*(\to D_s\pi)l\nu$ mode.

(iii) The angular observables such as A_3, A_4, A_5, A_{6s} are, however, quite different for both the decay modes. The central values obtained for A_3, A_4, and A_5 in $B_s \to D_s^*(\to D_s\pi)l\nu$ mode are twice as large as the values obtained in case of $B_s \to D_s^*(\to D_s\gamma)l\nu$ mode.

(iv) The angular observables A_7, A_8, and A_9 are zero in the SM and are nonvanishing only if NP induces a complex contribution to the amplitude.

(v) The ratio of branching ratio $R_{D_s^*}$ is found to be 0.2430 ± 0.0015 which is quite similar to the value reported in Ref. [100]. The authors in Ref. [100] calculate $R_{D_s^*}$ by considering the τ and the μ mode. However, in our paper, we have calculated $R_{D_s^*}$ using the τ and the e mode. The slight difference in $R_{D_s^*}$ is mainly coming from the mass of the lepton. Moreover, by considering the τ and the μ mode, we have obtained the value of $R_{D_s^*}$ to be 0.2442 ± 0.0015 where the central value is exactly same with the

TABLE III. The central values and the corresponding 1σ ranges of various observables in the SM.

	$B_s \to D_s^*(\to D_s\pi)l\nu$ decay mode		$B_s \to D_s^*(\to D_s\gamma)l\nu$ decay mode	
Observable	e-mode	τ mode	e mode	τ mode
BR	$(3.0516 \pm 0.0988) \times 10^{-3}$	$(0.7415 \pm 0.0231) \times 10^{-3}$	$(4.9194 \pm 0.1593) \times 10^{-2}$	$(1.1954 \pm 0.0372) \times 10^{-2}$
A^l_{FB}	-0.2640 ± 0.0031	-0.0896 ± 0.0020	-0.2640 ± 0.0031	-0.0896 ± 0.0020
A^T_{FB}	-0.5436 ± 0.0035	-0.3842 ± 0.0026	-0.5436 ± 0.0035	-0.3842 ± 0.0026
F_L	0.5143 ± 0.0040	0.4482 ± 0.0015	0.5143 ± 0.0040	0.4482 ± 0.0015
A_3	-0.0252 ± 0.0003	-0.0162 ± 0.0001	0.0126 ± 0.0001	0.0081 ± 0.0001
A_4	0.1909 ± 0.0005	0.0883 ± 0.0001	-0.0954 ± 0.0002	-0.0442 ± 0.0001
A_5	-0.2139 ± 0.0019	-0.2265 ± 0.0010	0.1069 ± 0.0010	0.1133 ± 0.0005
A_{6s}	1.1882 ± 0.0140	0.9539 ± 0.0077	-0.0000 ± 0.0000	-0.5509 ± 0.0026
C^l_F	-0.4071 ± 0.0091	-0.0550 ± 0.0014	-0.4071 ± 0.0091	-0.0550 ± 0.0014
A_7	0.0000	0.0000	0.0000	0.0000
A_8	0.0000	0.0000	0.0000	0.0000
A_9	0.0000	0.0000	0.0000	0.0000
$R_{D_s^*}$	0.2430 ± 0.0015		0.2430 ± 0.0015	

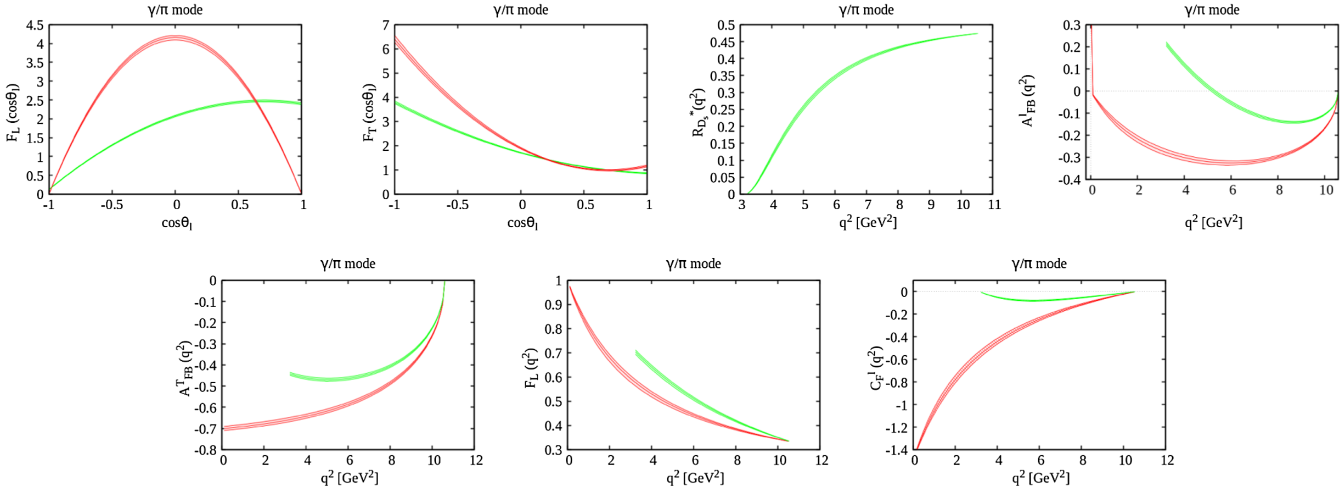

FIG. 1. q^2 and $\cos\theta_l$ dependence of $B_s \to D_s^*(\to D_s\gamma, D_s\pi)l\nu$ decay observables in the SM for the e (red) and the τ (green) mode.

central values obtained in [100]. We, however, observe a slight difference in the uncertainties associated with it.

In Fig. 1, we show several q^2 and $\cos\theta_l$ dependent observables such as $R_{D_s^*}(q^2)$, $A^l_{FB}(q^2)$, $A^T_{FB}(q^2)$, $F_L(q^2)$, $C^l_F(q^2)$, $F_L(\cos\theta_l)$, and $F_T(\cos\theta_l)$ for the $B_s \to D_s^*(\to D_s\gamma, D_s\pi)l\nu$ decay mode. It should be mentioned that these observables show exact same behavior for the $D_s\pi$ and the $D_s\gamma$ mode. Here the red color represents the e mode and green color represents the τ mode, respectively. Our main observations are as follows.

(i) $A^l_{FB}(q^2)$: We observe a zero crossing of $A^\tau_{FB}(q^2)$ at $q^2 = 5.25 \pm 0.10$ GeV^2.

(ii) $A^T_{FB}(q^2)$: $A^T_{FB}(q^2)$ is minimum at low q^2 and assumes negative values for the whole q^2 range in both e mode and τ mode. Moreover, it increases with q^2 and becomes zero at $q^2 = q^2_{\rm max}$.

(iii) $C^l_F(q^2)$: The convexity parameter $C^e_F(q^2)$ is found to be minimum at low q^2 and it increases as q^2 increases. At $q^2 = q^2_{\rm max}$, it is equal to zero for both e and the τ mode.

(iv) $F_L(q^2)$: The longitudinal polarization fraction $F_L(q^2)$ is maximum for low value of q^2. It gradually decreases and becomes minimum at $q^2 = q^2_{\rm max}$.

(v) $F_L(\cos\theta_l)$: The distribution is found to be symmetric in case of e mode but not for the τ mode. This is due to the presence of lepton mass term in the amplitude. At $\cos\theta_l = 0$, $F_L(\cos\theta_l)$ is maximum for e mode, whereas, for the τ mode, the maximum occurs at $\cos\theta_l = 1$.

(vi) $F_T(\cos\theta_l)$: The maximum value of F_T is obtained for $\cos\theta_l = -1$ for both e and the τ mode. it gradually decreases with increasing $\cos\theta_l$ and becomes minimum near $\cos\theta_l = 1$.

In Fig. 2, we display the q^2 and $\cos\theta_{D_s}$ dependence of several observables that are different for $B_s \to D_s^*(\to D_s\pi)l\nu$ and $B_s \to D_s^*(\to D_s\gamma)l\nu$ decay modes. Here the red color represents the e mode and green color represents the τ mode, respectively. Our observations are as follows.

(i) DBR: In case of $B_s \to D_s^*(\to D_s\gamma)l\nu$ decay mode, the maximum value of DBR $= (0.567 \pm 0.037) \times 10^{-2}$ is observed at $q^2 \approx 6.04$ GeV^2 for the e mode, whereas, the maximum value of DBR $= (0.241 \pm 0.015) \times 10^{-2}$ is observed at $q^2 \approx 8.28$ GeV^2 for the τ mode. Similarly, for $B_s \to D_s^*(\to D_s\pi)l\nu$, the DBR peak of $(0.351 \pm 0.023) \times 10^{-3}$ is observed at $q^2 \approx 6.15$ GeV^2 for e mode and maximum DBR $= (0.150 \pm 0.010) \times 10^{-3}$ is observed at $q^2 \approx 8.07$ GeV^2 for the τ mode.

(ii) $A_3(q^2), A_4(q^2), A_5(q^2)$: The angular observables A_is obey a strict relation $A^\pi_i = -2A^\gamma_i$ at all values of q^2 for the $D_s\pi$ and $D_s\gamma$ mode.

(iii) $A_{6s}(q^2)$: For the $D_s\gamma$ channel, $A_{6s}(q^2)$ is observed to be zero for the e mode, whereas, it is minimum at low q^2 and maximum at high q^2 for the τ mode. It should also be mentioned that value of A_{6s} is negative for the whole q^2 range. For the $D_s\pi$ channel, the maximum of A_{6s} is observed at $q^2 \approx 5.98$ GeV^2 for the e mode and it is observed at $q^2 \approx 7.28$ GeV^2 for the τ mode.

(iv) $F_L(\cos\theta_{D_s})$: The behavior of F_L is symmetric about $\cos\theta_{D_s}$. The maximum value of F_L is obtained at $\cos\theta_{D_s} = 0$ for both e and the τ mode in the $D_s\gamma$ mode, whereas, in $D_s\pi$ mode, we observe a minimum at $\cos\theta_{D_s} = 0$.

(v) $F_T(\cos\theta_{D_s})$: F_T is symmetric in $\cos\theta_{D_s}$ for both $D_s\gamma$ and $D_s\pi$ mode. F_T is minimum at $\cos\theta_{D_s} = 0$, whereas, it is found to be maximum at $\cos\theta_{D_s} = \pm 1$ for the $D_s\gamma$ mode. For the $D_s\pi$ mode, the maximum, however, occurs at $\cos\theta_{D_s} = 0$ and it goes to zero at $\cos\theta_{D_s} = \pm 1$.

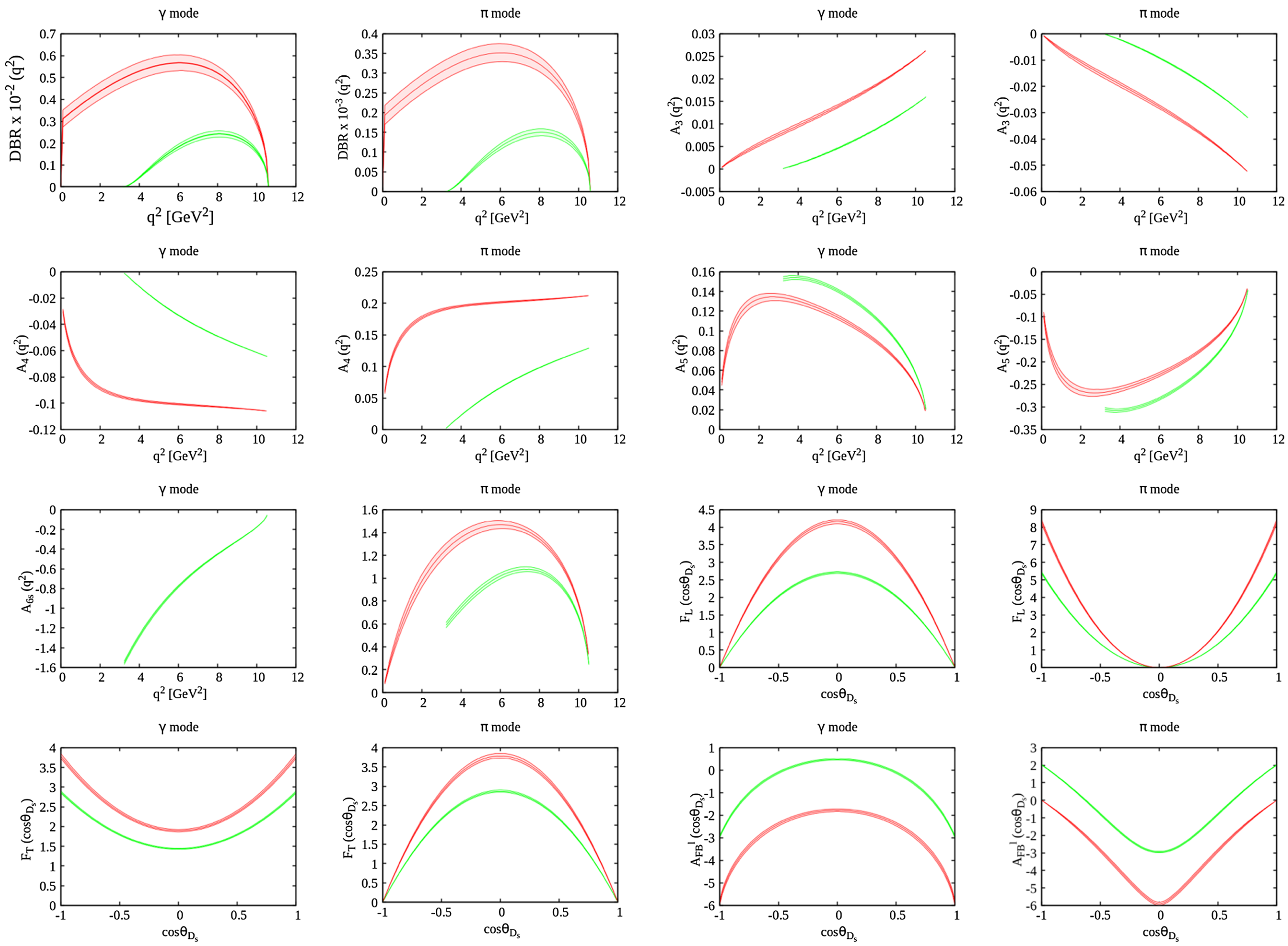

FIG. 2. q^2 and $\cos\theta_{D_s}$ dependence of $B_s \to D_s^*(\to D_s\gamma, D_s\pi)l\nu$ decay observables in the SM for the e (red) and the τ (green) mode.

(vi) $A^l_{FB}(\cos\theta_{D_s})$: $A^l_{FB}(\cos\theta_{D_s})$ is symmetric in $\cos\theta_{D_s}$ for both $D_s\gamma$ and $D_s\pi$ modes. For $D_s\gamma$ mode, $A^l_{FB}(\cos\theta_{D_s})$ is minimum at $\cos\theta = \pm 1$, whereas, it is maximum at $\cos\theta = 0$ for both e and the τ mode. However, for $D_s\pi$ mode, it is completely opposite. $A^l_{FB}(\cos\theta_{D_s})$ is maximum at $\cos\theta = \pm 1$ and minimum at $\cos\theta = 0$ for both e and the τ cases. It should also be mentioned that, a zero crossing in $A^\tau_{FB}(\cos\theta_{D_s})$ is observed at $\cos\theta_{D_s} = \pm 0.456 \pm 0.018$ for the $D_s\gamma$ mode, whereas, the zero crossing point is observed at $\cos\theta_{D_s} = \pm 0.626 \pm 0.007$ for the $D_s\pi$ mode.

The parametrization of the $B_s \to D_s^*$ form factors consists of a pole factor with no uncertainty and a polynomial in z for which the coefficients with their uncertainties are given in Table XIII of Ref. [100]. They also provide the correlations between the z-expansion coefficients which are necessary for reconstructing their results explicitly. In our error analysis, however, we have not considered the correlations between the z-expansion coefficients. Hence our errors are smaller than the errors reported in [100]. The parametrization of the $B_s \to D_s^*$ form factors consists of a pole factor with no uncertainty and a polynomial in z for which the coefficients with their uncertainties are given in Table XIII of [100]. They also provide the correlations between the z-expansion coefficients which are necessary for reconstructing their results explicitly. In our error analysis, however, we have not considered the correlations between the z-expansion coefficients. Hence our errors are smaller than the errors reported in [100].

C. New physics analysis

We now proceed to discuss the NP effects on various physical observables in the angular distribution of $B_s \to D_s^*(\to D_s\gamma)\tau\nu$ and $B_s \to D_s^*(\to D_s\pi)\tau\nu$ decays in a model independent framework. We have taken three possible NP scenarios. The best fit values of the NP couplings under each scenarios, taken from recent global fit analysis [61,82,83], are reported in Table IV.

1. Scenario I

In scenario I, we choose four different 1D NP hypothesis and the corresponding best fit values of Refs. [82,83]

TABLE IV. Best fit value of NP couplings.

New physics scenarios		
Scenerio—I [82,83]	Scenerio—II [82,83]	Scenerio—III [61]
$g_{V_L} = 0.07$	$(g_{V_L}, g_{S_L} = -4g_{T_L}) = (0.10, -0.04)$	$g_{V_L} = 0.07 - i0.16$
$g_{S_R} = 0.09$	$(g_{S_R}, g_{S_L}) = (0.21, -0.15)(SetA)$ or	$g_{V_R} = -0.01 - i0.39$
$g_{S_L} = 0.07$	$(g_{S_R}, g_{S_L}) = (-0.26, -0.61)(SetB)$	$g_{S_L} = 0.29 - i0.67$
$g_{S_L} = 4g_{T_L} = -0.03$	$(g_{V_L}, g_{S_R}) = (0.08, -0.01)$	$g_{S_R} = 0.19 + i0.08$
	$(g_{S_L} = 4g_{T_L}) = (-0.06 + i0.31)$	$g_{T_L} = 0.11 - i0.18$

obtained at scale $\mu = 1$ TeV are reported in Table IV. For our analysis, we run these NP couplings down to the renormalization scale $\mu = m_b$ [82,83]. The effect of these NP couplings on several physical observables pertaining to $B_s \to D_s^*(\to D_s\gamma)\tau\nu$ and $B_s \to D_s^*(\to D_s\pi)\tau\nu$ decay modes are reported in Table V.

It is clear from from Table V that in the presence of g_{V_L} NP coupling, the branching ratio gets considerable deviations from the SM predication. However, no deviation from the SM prediction is observed for observables that are in the form of ratios. The NP dependency cancels in these ratios. In the presence of g_{S_L}, g_{S_R} and $g_{S_L} = 4g_{T_L}$ NP couplings, A_{FB}^τ is found to be at more than 4σ away from the SM prediction for both $D_s\gamma$ and $D_s\pi$ mode. Similarly, a deviation of around 3.4σ, 4.71σ and 1σ is observed for F_L in the presence of g_{S_L}, g_{S_R} and $g_{S_L} = 4g_{T_L}$ NP couplings. Moreover, the deviation from the SM expectation observed in case of $R_{D_s^*}$ is at the level of 2.05σ and 3.83 significance in the presence of g_{S_R} and $g_{S_L} = 4g_{T_L}$ NP couplings respectively, whereas, it is at the level of 15σ significance for g_{V_L} NP coupling. The observables A_3 and A_{FB}^T show slight deviation from the SM in the presence of $g_{S_L} = 4g_{T_L}$ NP coupling. As expected, A_7, A_8 and A_9 are all zero and hence we do not report them in Table V.

In Fig 3 we display the q^2 and $\cos\theta_l$ dependence of several physical observables that exhibit same behavior for the $D_s\gamma$ and $D_s\pi$ modes. The contribution coming from $g_{V_L}, g_{S_L}, g_{S_R}, g_{S_L} = 4g_{T_L}$ NP couplings are represented by blue, black, violet, and orange lines and band respectively. Our observations are as follows.

(i) In case of $F_L(\cos\theta_l)$, a slight deviation from SM expectation is observed at $\cos\theta_l \geq 0.5$ with g_{S_L} and g_{S_R} NP couplings and they are distinguishable from the SM prediction at slightly more than 1σ significance. However, for $F_T(\cos\theta_l)$, no such deviation is observed and they all lie within the SM error band.

(ii) In case of $R_{D_s^*}(q^2)$, maximum deviation is observed in case of g_{V_L} NP coupling and it is clearly distinguishable from the SM prediction at more than 3σ significance at high q^2 value.

(iii) The zero crossing in $A_{FB}^\tau(q^2)$ is shifted to lower value of q^2 than in the SM with g_{S_L} NP coupling, whereas, it is found to be shifted to higher value of q^2 with g_{S_R} and $g_{S_L} = 4g_{T_L}$ NP couplings. The zero crossings in A_{FB}^τ at $q^2 = 5.06\ \mathrm{GeV}^2 \pm 0.2$, $q^2 = 5.48\ \mathrm{GeV}^2 \pm 0.11$ and $q^2 = 5.43\ \mathrm{GeV}^2 \pm 0.10$ in the presence of g_{S_L}, g_{S_R}, and $g_{S_L} = 4g_{T_L}$ NP couplings are clearly distinguishable from the SM prediction of $q^2 = 5.25 \pm 0.10\ \mathrm{GeV}^2$ at the level of 0.85σ and 1.54σ and 1.27σ significance.

(iv) At low q^2 range, $A_{FB}^T(q^2)$ deviates from the SM predication in the presence of $g_{S_L} = 4g_{T_L}$ NP coupling. In case of $F_L(q^2)$ and $C_F^\tau(q^2)$ observables,

TABLE V. Prediction of $B_s \to D_s^*(\to D_s\gamma, D_s\pi)\tau\nu$ decay observables in Scenario I.

	g_{V_L}		g_{S_L}		g_{S_R}		$g_{S_L} = 4g_{T_L}$	
	$D_s\gamma$	$D_s\pi$	$D_s\gamma$	$D_s\pi$	$D_s\gamma$	$D_s\pi$	$D_s\gamma$	$D_s\pi$
$BR \times 10^{-2}$	1.3686 ± 0.0426	0.0849 ± 0.0026	1.1798 ± 0.0367	0.0732 ± 0.0023	1.2174 ± 0.0379	0.0755 ± 0.0024	1.2382 ± 0.0392	0.0768 ± 0.0024
A_3	0.0081 ± 0.0001	-0.0162 ± 0.0001	0.0082 ± 0.0001	-0.0164 ± 0.0001	0.0080 ± 0.0001	-0.0159 ± 0.0001	0.0078 ± 0.0001	-0.0156 ± 0.0002
A_4	-0.0442 ± 0.0001	0.0883 ± 0.0001	-0.0448 ± 0.0001	0.0895 ± 0.0001	-0.0434 ± 0.0001	0.0867 ± 0.0001	-0.0426 ± 0.0001	0.0852 ± 0.0001
A_5	0.1133 ± 0.0005	-0.2265 ± 0.0010	0.1104 ± 0.0005	-0.2208 ± 0.0010	0.1166 ± 0.0005	-0.2333 ± 0.0010	0.1119 ± 0.0005	-0.2238 ± 0.0010
A_{6s}	-0.5509 ± 0.0026	0.9539 ± 0.0077	-0.5076 ± 0.0025	0.9665 ± 0.0078	-0.6033 ± 0.0028	0.9366 ± 0.0076	-0.5673 ± 0.0028	0.9098 ± 0.0078
$R_{D_s^*}$	0.2782 ± 0.0018		0.2398 ± 0.0015		0.2475 ± 0.0016		0.2517 ± 0.0017	
A_{FB}^τ	-0.0896 ± 0.0020		-0.1020 ± 0.0020		-0.0741 ± 0.0021		-0.0761 ± 0.0021	
A_{FB}^T	-0.3842 ± 0.0026		-0.3842 ± 0.0026		-0.3842 ± 0.0026		-0.3677 ± 0.0026	
F_L	0.4482 ± 0.0015		0.4409 ± 0.0015		0.4582 ± 0.0015		0.4501 ± 0.0016	
C_F^l	-0.0550 ± 0.0014		-0.0557 ± 0.0014		-0.0540 ± 0.0014		-0.0531 ± 0.0014	

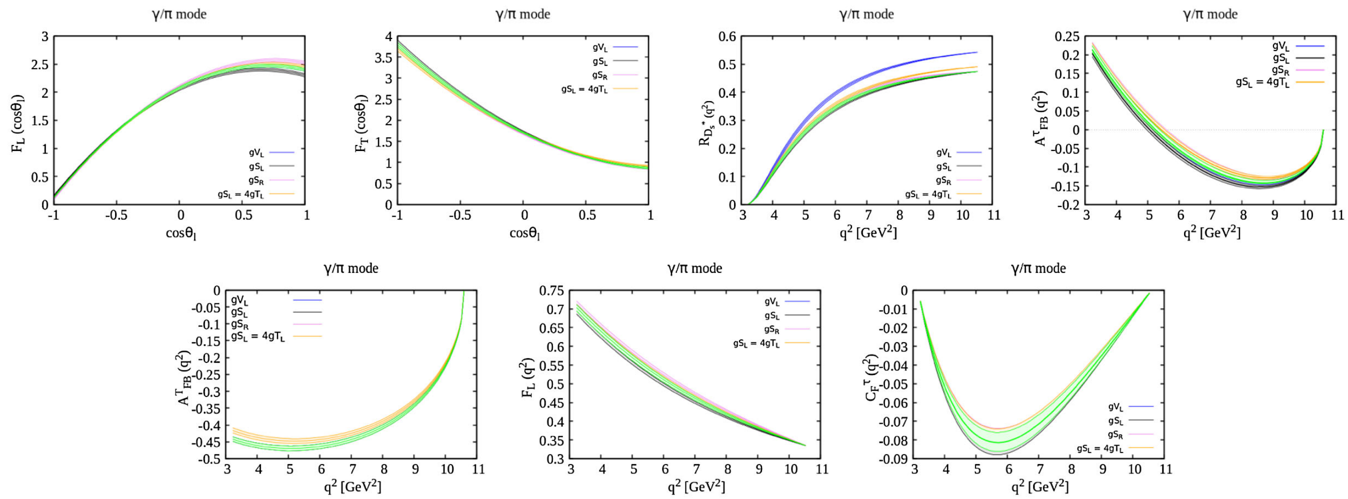

FIG. 3. The q^2 and $\cos\theta_l$ dependence of $B_s \to D_s^*(\to D_s\gamma, D_s\pi)\tau\nu$ decay observables in the SM and in the presence of the NP couplings of scenario I. The SM central line and the corresponding error band are shown with green color. The blue, black, violet, and orange lines and bands represent the effect of $g_{V_L}, g_{S_L}, g_{S_R}, g_{S_L} = 4g_{T_L}$ NP couplings, respectively.

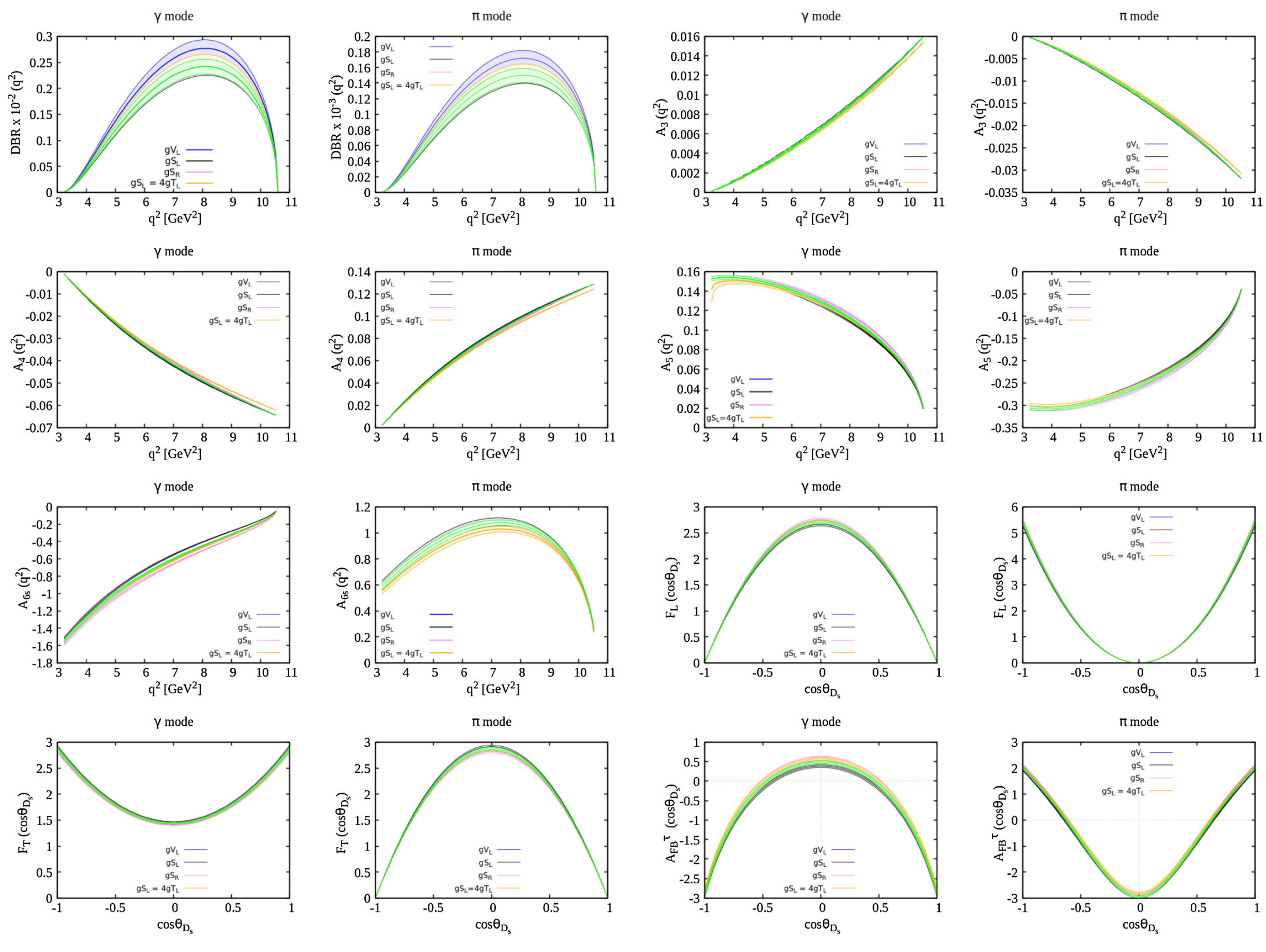

FIG. 4. The q^2 and $\cos\theta_{D_s}$ dependence of various physical observable of $B_s \to D_s^*(\to D_s\gamma, D_s\pi)\tau\nu$ in the SM and in the presence of the NP couplings of scenario I. The SM central line and the corresponding error band are shown with green color. The blue, black, violet, and orange colors represents the effect of NP coupling $g_{V_L}, g_{S_L}, g_{S_R}, g_{S_L} = 4g_{T_L}$ respectively.

no significant deviation is observed and they all lie within the SM error band.

In Fig. 4 we display the q^2 and $\cos\theta_{D_s}$ dependence of several physical observables that exhibits different behavior for the $D_s\gamma$ and $D_s\pi$ decay modes. Our observations are as follows.

(i) In case of differential branching ratio $\mathrm{DBR}(q^2)$, the deviation from the SM prediction is more pronounced with g_{V_L} NP coupling and the peak of the distribution is clearly distinguishable from the SM prediction at the level of 2σ significance. No such significant deviation is observed with the rest of the NP couplings and they all lie within the SM error band.

(ii) The angular observable A_3, A_4 and A_5 are slightly deviated from the SM in the presence of $g_{S_L} = 4g_{T_L}$ NP coupling. Similarly in case of A_{6s}, a slight deviation is observed with g_{S_L}, g_{S_R} and $g_{S_L} = 4g_{T_L}$ NP coupling for the $D_s\gamma$ mode, whereas, A_{6s} shows slight deviation in the presence of $g_{S_L} = 4g_{T_L}$ for the $D_s\pi$ mode.

(iii) The observables $F_L(\cos\theta_{D_s})$ and $F_T(\cos\theta_{D_s})$ do not show any significant deviation from the SM prediction in the presence of the NP couplings of scenario I.

(iv) The deviation from the SM prediction observed in case of $A^{\tau}_{FB}(\cos\theta_{D_s})$ is more pronounced with g_{S_L}, g_{S_R} and $g_{S_L} = 4g_{T_L}$ NP couplings for the $D_s\gamma$ mode. The zero crossing in $A^{\tau}_{FB}(\cos\theta_{D_s})$ is shifted to $\cos\theta_{D_s} = 0.412 \pm 0.02, 0.500 \pm 0.016$ and 0.497 ± 0.018 in the presence of g_{S_L}, g_{S_R}, and $g_{S_L} = 4g_{T_L}$ NP couplings and they are clearly distinguishable from the SM zero crossing of $\cos\theta_{D_s} = \pm 0.456 \pm 0.018$ at the level of more than 1.5σ significance. Similarly for the $D_s\pi$ mode, $A^{\tau}_{FB}(\cos\theta_{D_s})$ shows slight deviation in the presence of g_{S_L}, g_{S_R}, and $g_{S_L} = 4g_{T_L}$ NP couplings. The zero crossings in $A^{\tau}_{FB}(\cos\theta_{D_s})$ observed at $\cos\theta_{D_s} = \pm 0.642 \pm 0.005$, $\pm 0.610 \pm 0.007$, and $\pm 0.613 \pm 0.007$ in the presence of g_{S_L}, g_{S_R}, and $g_{S_L} = 4g_{T_L}$ NP couplings are distinguishable from the SM zero crossing of $\cos\theta_{D_s} = \pm 0.626 \pm 0.007$ at the level of more than 1.2σ significance.

2. (Scenario II)

In scenario II, we choose four 2D NP hypothesis such as (g_{V_L}, $g_{S_L} = -4g_{T_L}$), (g_{S_R}, g_{S_L}) (Set A or Set B), (g_{V_L}, g_{S_R}) and ($g_{S_L} = 4g_{T_L}$). The best fit values of these NP couplings at $\mu = 1$ TeV scale obtained from Refs. [82,83] are mentioned in the Table IV. In our analysis, we run them down to the renormalization scale of $\mu = m_b$. In Table VI, we report the central values and the corresponding 1σ range of several physical observables for both $B_s \to D_s^*(\to D_s\gamma)\tau\nu$ and $B_s \to D_s^*(\to D_s\pi)\tau\nu$ decays in the presence of each $2D$ NP couplings.

TABLE VI. Prediction of $B_s \to D_s^*(\to D_s\gamma, D_s\pi)\tau\nu$ decay observables in Scenario II.

	$(g_{V_L}, g_{S_L} = -4g_{T_L})$		(g_{S_R}, g_{S_L}) (Set A)		(g_{S_R}, g_{S_L}) (Set B)		(g_{V_L}, g_{S_R})		$g_{S_L} = 4g_{T_L}$	
	$D_s\gamma$	$D_s\pi$	$D_s\gamma$	$D_s\pi$	$D_s\gamma$	$D_s\pi$	$D_s\gamma$	$D_s\pi$	$D_s\gamma$	$D_s\pi$
$BR \times 10^{-2}$	1.4049 ± 0.0444	0.0872 ± 0.0027	1.2984 ± 0.0404	0.0805 ± 0.0025	1.2963 ± 0.0404	0.0804 ± 0.0025	1.3918 ± 0.0433	0.0863 ± 0.0027	1.3696 ± 0.0426	0.0850 ± 0.0026
A_3	0.0083 ± 0.0001	-0.0167 ± 0.0002	0.0075 ± 0.0001	-0.0149 ± 0.0001	0.0075 ± 0.0001	-0.0150 ± 0.0001	0.0081 ± 0.0001	-0.0162 ± 0.0001	0.0066 ± 0.0001	-0.0132 ± 0.0002
A_4	-0.0454 ± 0.0001	0.0909 ± 0.0002	-0.0407 ± 0.0001	0.0813 ± 0.0002	-0.0407 ± 0.0001	0.0815 ± 0.0002	-0.0443 ± 0.0001	0.0885 ± 0.0001	-0.0359 ± 0.0001	0.0719 ± 0.0002
A_5	0.1178 ± 0.0005	-0.2356 ± 0.0010	0.1247 ± 0.0004	-0.2493 ± 0.0009	0.1245 ± 0.0004	-0.2490 ± 0.0009	0.1129 ± 0.0005	-0.2258 ± 0.0010	0.1084 ± 0.0005	-0.2168 ± 0.0010
A_{6s}	-0.5736 ± 0.0029	0.9950 ± 0.0078	-0.7422 ± 0.0030	0.8782 ± 0.0072	-0.7394 ± 0.0030	0.8796 ± 0.0072	-0.5453 ± 0.0026	0.9556 ± 0.0078	-0.6032 ± 0.0030	0.7508 ± 0.0076
A_7	0.0000		0.0000		0.0000		0.0000		0.0086 ± 0.0004	0.0172 ± 0.0007
$R_{D_s^*}$	0.2856 ± 0.0019		0.2639 ± 0.0018		0.2635 ± 0.0018		0.2829 ± 0.0018		0.2784 ± 0.0019	
A^{τ}_{FB}	-0.0936 ± 0.0021		-0.0302 ± 0.0021		-0.0311 ± 0.0021		-0.0912 ± 0.0020		-0.0328 ± 0.0020	
A^{T}_{FB}	-0.4047 ± 0.0025		-0.3842 ± 0.0026		-0.3842 ± 0.0026		-0.3842 ± 0.0026		-0.3000 ± 0.0027	
F_L	0.4537 ± 0.0017		0.4920 ± 0.0015		0.4912 ± 0.0015		0.4472 ± 0.0015		0.4438 ± 0.0015	
C^l_F	-0.0567 ± 0.0015		-0.0506 ± 0.0013		-0.0507 ± 0.0013		-0.0551 ± 0.0014		-0.0559 ± 0.0013	

The deviation from the SM prediction observed for BR is more pronounced in the presence of $(g_{V_L}, g_{S_L} = -4g_{T_L})$ and $(g_{S_L} = 4g_{T_L})$ NP coupling and it is clearly distinguishable from the SM prediction at more than 3σ significance. Similarly, a deviation of around $2-3\sigma$ is observed with (g_{S_R}, g_{S_L}) (set A or set B) and (g_{V_L}, g_{S_R}) NP couplings. Significant deviation from the SM prediction is observed for $R_{D_s^*}$ with all NP couplings. The observable A^τ_{FB} lies more than 10σ away from the SM expectation in the presence of (g_{S_R}, g_{S_L}) (set A or Set B) and $(g_{S_L} = 4g_{T_L})$ NP couplings. Similarly, the observable A^T_{FB} deviates at more than 10σ significance from the SM expectation in the presence of $(g_{S_L} = 4g_{T_L})$ NP coupling. In case of F_L, the deviation is more pronounced with (g_{S_R}, g_{S_L}) (set A or set B) NP couplings. A deviation of more than 2σ is observed for C^τ_F in the presence of (g_{S_R}, g_{S_L}) (set A or set B) NP coupling. The angular observable A_7 is found to be nonzero in the presence of $(g_{S_L} = 4g_{T_L})$ complex NP couplings for both $D_s\gamma$ and $D_s\pi$ modes. The angular observables A_8 and A_9 are absent in this scenario II and hence we do not report them in Table VI.

We display the q^2 and $\cos\theta_l$ dependence of several physical observables that show same behavior for the $D_s\gamma$ and $D_s\pi$ decay modes in Fig. 5. The blue, black, yellow, violet, and red lines and its corresponding bands represent the contribution coming from $(g_{V_L}, g_{S_L} = -4g_{T_L})$, (g_{S_R}, g_{S_L}) (Set A), (g_{S_R}, g_{S_L}) (Set B), (g_{V_L}, g_{S_R}), and $(g_{S_L} = 4g_{T_L})$ NP couplings, respectively. Our observations are as follows.

(i) Although a slight deviation from the SM prediction is observed for $F_L(\cos\theta_l)$ with $(g_{S_L} = 4g_{T_L})$ NP coupling, the deviation, however, is quite significant in the presence of (g_{S_R}, g_{S_L}) (Set A or Set B) NP couplings. Similarly, $F_T(\cos\theta_l)$ is observed to be deviated from the corresponding SM value in the presence of (g_{S_R}, g_{S_L}) (Set A or Set B) and $(g_{S_L} = 4g_{T_L})$ NP couplings.

(ii) Although the deviation from the SM prediction for $R_{D_s^*}(q^2)$ is quite significant for all the $2D$ NP couplings, it is more pronounced in case of $(g_{V_L}, g_{S_L} = -4g_{T_L})$, (g_{V_L}, g_{S_R}) and $(g_{S_L} = 4g_{T_L})$ NP couplings and they are clearly distinguishable from the SM prediction at more than 10σ significance.

(iii) The zero crossing in $A^\tau_{FB}(q^2)$ is shifted to higher value of q^2 than in the SM in the presence of (g_{S_R}, g_{S_L}) (Set A or Set B) and $(g_{S_L} = 4g_{T_L})$ NP couplings. The zero crossings of $A^\tau_{FB}(q^2)$ at $q^2 = 6.28 \pm 0.125$ GeV^2 and $q^2 = 6.16 \pm 0.13$ GeV^2 in the presence of these NP couplings are clearly distinguishable from the SM prediction of $q^2 = 5.25 \pm 0.10$ GeV^2 at more than 5σ significance. Similarly, for $A^T_{FB}(q^2)$, a significant deviation of more than 10σ is observed at low q^2 in the presence of $g_{S_L} = 4g_{T_L}$ NP coupling.

(iv) In case of $F_L(q^2)$, although a slight deviation is observed with $(g_{S_L} = 4g_{T_L})$ NP coupling, the deviation, however, is more pronounced in the presence of (g_{S_R}, g_{S_L}) (Set A or Set B) NP couplings. Similarly for $C^\tau_F(q^2)$, maximum deviation from the SM prediction is observed with (g_{S_R}, g_{S_L}) (Set A or Set B) NP couplings.

The q^2 and $\cos\theta_{D_s}$ dependent observables which exhibit different behavior for $D_s\pi$ and $D_s\gamma$ modes are displayed in Fig 6. The left panel figures correspond to the $D_s\gamma$ mode and right panel figures correspond to the $D_s\pi$ mode, respectively. Our observations are as follows.

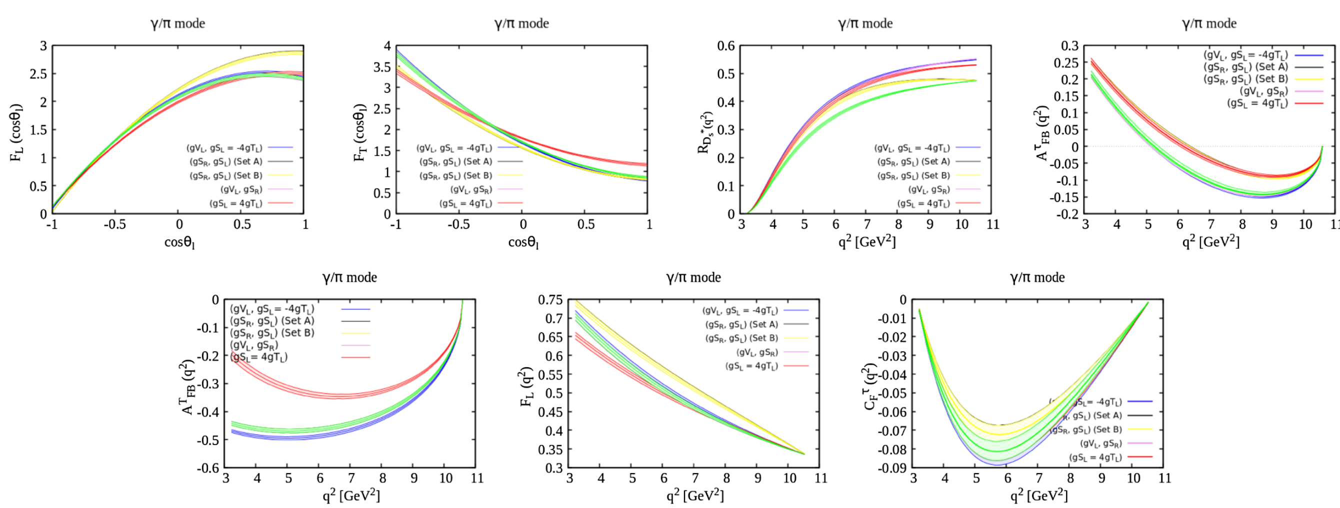

FIG. 5. The q^2 and $\cos\theta_l$ dependence of various physical observable of $B_s \to D_s^*(\to D_s\gamma, D_s\pi)\tau\nu$ in the SM and in the presence of the NP couplings of scenario II. The SM central line and the corresponding error band are shown with green color. The blue, black, yellow, violet, and red color colors represents the effect of NP coupling $(g_{V_L}, g_{S_L} = -4g_{T_L})$, (g_{S_R}, g_{S_L}) (Set A), (g_{S_R}, g_{S_L}) (Set B), (g_{V_L}, g_{S_R}), and $(g_{S_L} = 4g_{T_L})$ respectively.

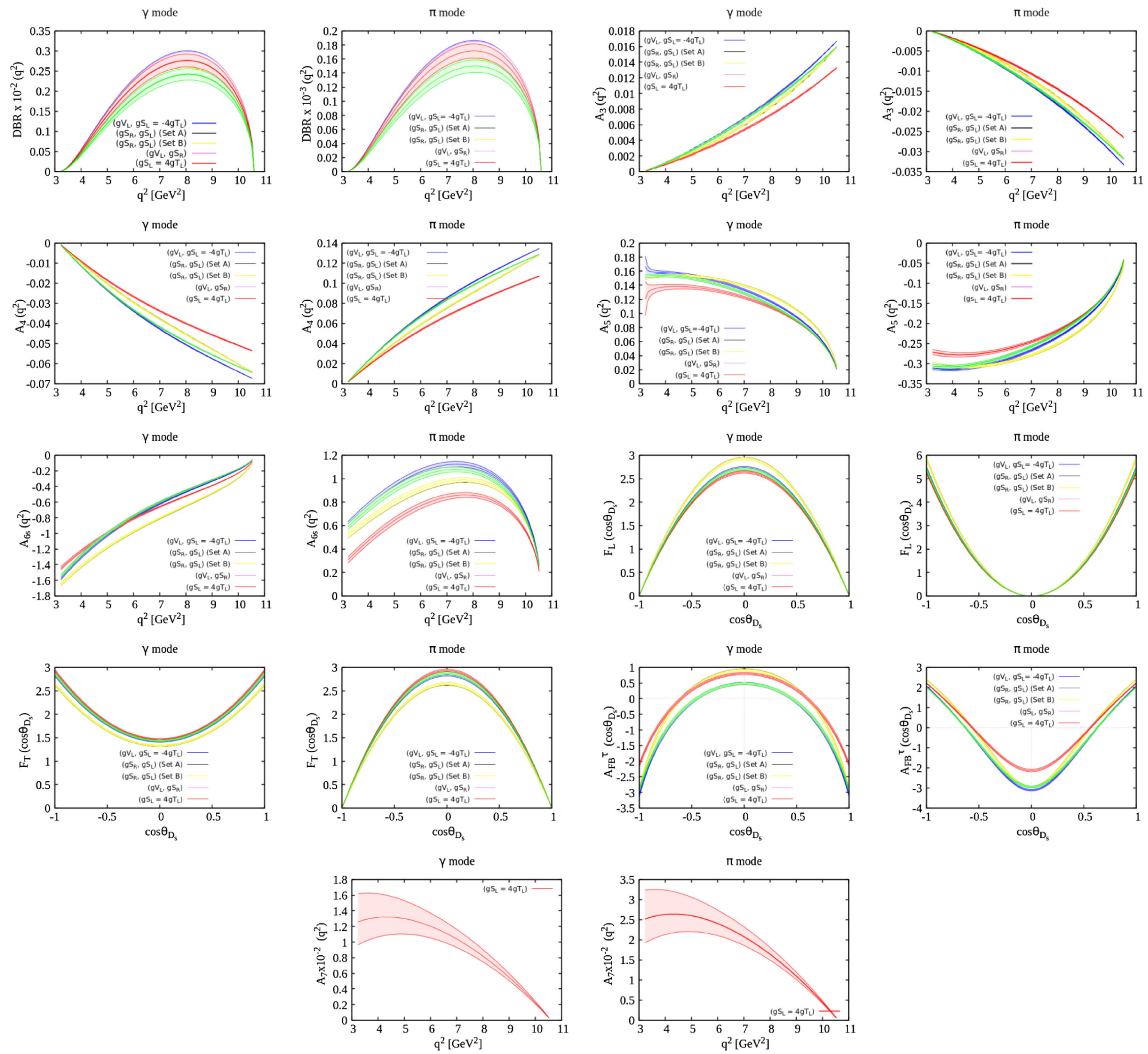

FIG. 6. The q^2 and $\cos\theta_{D_s}$ dependence of various physical observable of $B_s \to D_s^*(\to D_s\gamma, D_s\pi)\tau\nu$ in the SM and in the presence of the NP couplings of scenario II. The SM central line and the corresponding error band are shown with green color. The blue, black, yellow, violet, and red color colors represents the effect of NP coupling $(g_{V_L}, g_{S_L} = -4g_{T_L})$, (g_{S_R}, g_{S_L}) (Set A), (g_{S_R}, g_{S_L}) (Set B), (g_{V_L}, g_{S_R}) and $(g_{S_L} = 4g_{T_L})$ respectively.

(i) In case of $\mathrm{DBR}(q^2)$, although there is deviation from the SM prediction with all NP couplings, the deviation, however, is more pronounced once the $(g_{V_L}, g_{S_L} = -4g_{T_L})$ NP coupling is switched on and it is clearly distinguishable from the SM prediction at more than 3σ significance level.

(ii) For the A_3, A_4, and A_5 observables, the maximum deviation is observed in case of $(g_{S_L} = 4g_{T_L})$ NP couplings for both $D_s\pi$ and $D_s\gamma$ modes. For A_{6s}, the maximum deviation is observed with (g_{S_R}, g_{S_L}) (Set A or Set B) for the $D_s\gamma$ mode, whereas, for the $D_s\pi$ mode, the maximum deviation is observed with $(g_{S_L} = 4g_{T_L})$ NP coupling.

(iii) For the $D_s\gamma$ mode, $F_L(\cos\theta_{D_s})$ deviates significantly from the SM prediction at $\cos\theta_{D_s} = 0$ in the presence of (g_{S_R}, g_{S_L}) (Set A or Set B) NP coupling and it is clearly distinguishable from the SM error band, whereas, for the $D_s\pi$ mode, $F_L(\cos\theta_{D_s})$ shows a significant deviation at $\cos\theta_{D_s} = \pm 1$. In case of $F_T(\cos\theta_{D_s})$, the deviation from the SM prediction is more pronounced with (g_{S_R}, g_{S_L}) (Set A or Set B) NP couplings for both $D_s\pi$ and $D_s\gamma$ modes.

TABLE VII. Prediction of $B_s \to D_s^*(\to D_s\gamma, D_s\pi)\tau\nu$ decay observables in Scenario III.

	g_{V_L}		g_{V_R}		g_{S_L}		g_{S_R}		g_{T_L}	
	$D_s\gamma$	$D_s\pi$	$D_s\gamma$	$D_s\pi$	$D_s\gamma$	$D_s\pi$	$D_s\gamma$	$D_s\pi$	$D_s\gamma$	$D_s\pi$
$BR\times10^{-2}$	1.3992 ± 0.0436	0.0868 ± 0.0027	1.3980 ± 0.0435	0.0867 ± 0.0027	1.1831 ± 0.0368	0.0734 ± 0.0023	1.2228 ± 0.0381	0.0759 ± 0.0024	1.3681 ± 0.0439	0.0849 ± 0.0027
A_3	0.0081 ± 0.0001	-0.0162 ± 0.0001	0.0082 ± 0.0001	-0.0163 ± 0.0001	0.0082 ± 0.0001	-0.0164 ± 0.0001	0.0079 ± 0.0001	-0.0159 ± 0.0001	0.0019 ± 0.0001	-0.0038 ± 0.0003
A_4	-0.0442 ± 0.0001	0.0883 ± 0.0001	-0.0443 ± 0.0001	0.0886 ± 0.0001	-0.0446 ± 0.0001	0.0893 ± 0.0001	-0.0432 ± 0.0001	0.0864 ± 0.0001	-0.0112 ± 0.0005	0.0224 ± 0.0011
A_5	0.1133 ± 0.0005	-0.2265 ± 0.0010	0.0949 ± 0.0004	-0.1899 ± 0.0007	0.1041 ± 0.0005	-0.2082 ± 0.0010	0.1173 ± 0.0005	-0.2346 ± 0.0010	0.0566 ± 0.0012	-0.1132 ± 0.0024
A_{6s}	-0.5509 ± 0.0026	0.9539 ± 0.0077	-0.5521 ± 0.0026	0.6915 ± 0.0056	-0.4374 ± 0.0022	0.9638 ± 0.0078	-0.6141 ± 0.0028	0.9325 ± 0.0076	-0.2392 ± 0.0056	0.3422 ± 0.0095
A_7	0.0000		-0.0130 ± 0.0001	-0.0260 ± 0.0003	-0.0095 ± 0.0001	-0.0190 ± 0.0002	-0.0011 ± 0.0001	-0.0022 ± 0.0001	-0.0062 ± 0.0010	-0.0124 ± 0.0020
A_8	0.0000		-0.0102 ± 0.0001	-0.0205 ± 0.0002	0.0000		0.0000		0.0000	
A_9	0.0000		-0.0042 ± 0.0001	-0.0083 ± 0.0001	0.0000		0.0000		0.0000	
$R_{D_s^*}$	0.2844 ± 0.0018		0.2842 ± 0.0018		0.2405 ± 0.0015		0.2486 ± 0.0028		0.2781 ± 0.0028	
A_{FB}^{τ}	-0.0896 ± 0.0020		-0.0310 ± 0.0016		-0.1170 ± 0.0020		-0.0708 ± 0.0021		-0.0229 ± 0.0018	
A_{FB}^{T}	-0.3842 ± 0.0026		-0.2790 ± 0.0019		-0.3842 ± 0.0026		-0.3842 ± 0.0026		-0.1124 ± 0.0033	
F_L	0.4482 ± 0.0015		0.4493 ± 0.0015		0.4425 ± 0.0015		0.4606 ± 0.0015		0.3237 ± 0.0025	
C_F^l	-0.0550 ± 0.0014		-0.0558 ± 0.0014		-0.0555 ± 0.0014		-0.0537 ± 0.0014		-0.1316 ± 0.0026	

(iv) For $D_s\gamma$ and $D_s\pi$ mode, $A_{FB}^{\tau}(\cos\theta_{D_s})$ deviates significantly from the SM prediction in the presence of (g_{S_R}, g_{S_L}) (Set A or Set B) and $(g_{S_L} = 4g_{T_L})$ NP couplings. In the presence of (g_{S_R}, g_{S_L}) (Set A or Set B) and $(g_{S_L} = 4g_{T_L})$ NP couplings, the zero crossings in $A_{FB}^{\tau}(\cos\theta_{D_s})$ is observed at $\cos\theta_{D_s} = \pm0.601\pm0.012$ and $\cos\theta_{D_s} = \pm0.601\pm0.015$ for the in $D_s\gamma$ mode and at $\cos\theta_{D_s} = \pm0.563\pm0.007$ and $\cos\theta_{D_s} = \pm0.563\pm0.009$ for the $D_s\pi$ modes. Hence in each case the zero crossing point lie at 5σ away from the SM zero crossing point.

(v) We observe a non-zero q^2 distribution of $A_7(q^2)$ in the presence of $(g_{S_L} = 4g_{T_L})$ complex NP couplings.

3. (Scenario III)

In this scenario, we select five different complex $1D$ NP couplings. The best fit values each NP couplings at renormalization scale $\mu = m_b$ obtained from Ref. [61] are reported in Table IV. In Table VII, we report the impact of each NP couplings on various physical observable in $D_s\gamma$ and $D_s\pi$ decay modes. We see significant deviation of all the observables with these complex NP couplings. In the presence of g_{V_L}, g_{V_R}, and g_{T_L} NP couplings, branching ratio deviates from the SM prediction at the level of $3-6\sigma$ significance. A_{FB}^{τ} deviates more than 3σ in the presence of g_{V_R}, g_{S_L}, and g_{T_L} NP couplings and the observable A_{FB}^{T} deviates more than 10σ from the SM expectation in case of g_{V_R} and g_{T_L} NP coupling. Similarly, the longitudinal polarization fraction of D_s^*, F_L is found to deviate from the SM value at more than 10σ significance in the presence of g_{T_L} NP coupling for both the decay modes. In case of $R_{D_s^*}$, we observe a considerable deviation of around 10σ in the presence of g_{V_L}, g_{V_R}, and g_{T_L} NP couplings. The observable C_F^{τ} lies more than 10σ away from the SM in the presence of g_{T_L} NP coupling. Moreover, for A_3, A_4, and A_5 the maximum deviation from the SM prediction is observed with g_{T_L} NP coupling. For the angular observable A_{6s}, the deviation observed is more pronounced in case of g_{S_L}, g_{S_R}, and g_{T_L} NP couplings in $D_s\gamma$ mode, whereas, g_{V_R} and g_{T_L} show more significant deviation in case of $D_s\pi$ mode. A nonzero value of A_7 is also observed in the presence of g_{S_L}, g_{S_R}, and g_{T_L} NP couplings. The angular observables A_8 and A_9 assume nonzero values once g_{V_R} NP coupling is switched on. It should also be mentioned that the values of A_7, A_8, and A_9 in $D_s\pi$ mode is twice as large as the values obtained for the $D_s\gamma$ mode.

In Fig. 7 we show the q^2 and $\cos\theta_l$ dependence of various physical observables that exhibit same behavior for the $D_s\gamma$ and $D_s\pi$ modes. NP contribution coming from g_{V_L}, g_{V_R}, g_{S_L}, g_{S_R}, and g_{T_L} complex NP couplings are shown with blue, red, black, violet, and orange colored lines and bands, respectively. Our observations are as follows.

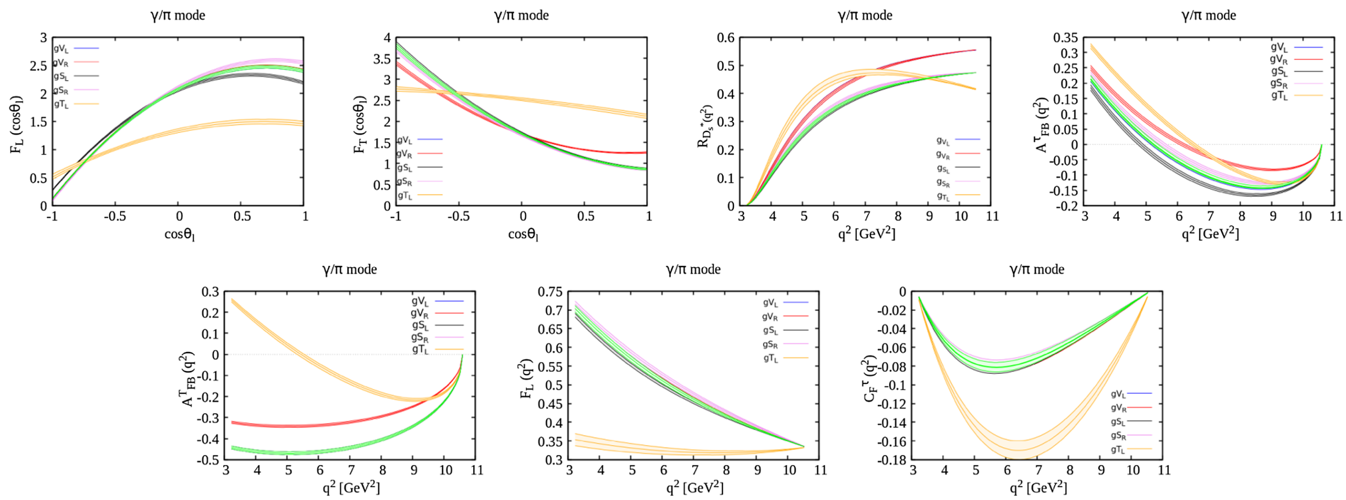

FIG. 7. The q^2 and $\cos\theta_l$ dependence of various physical observable of $B_s \to D_s^*(\to D_s\gamma, D_s\pi)\tau\nu$ in the SM and in the presence of the NP couplings of scenario III. The SM central line and the corresponding error band are shown with green color. The blue, red, black, violet, and orange colors represents the effect of NP coupling g_{V_L}, g_{V_R}, g_{S_L}, g_{S_R}, and g_{T_L} respectively.

(i) In the case of $F_L(\cos\theta_l)$, a significant deviation from the SM prediction is observed due to g_{T_L} NP coupling and it is quite distinct from the rest of NP couplings. Similarly, we observe significant deviation in $F_T(\cos\theta_l)$ once g_{V_R} and g_{T_L} NP couplings are switched on. Again, the behavior of $F_T(\cos\theta_l)$ is quite distinct with g_{T_L} NP coupling.

(ii) In case of $R_{D_s^*}(q^2)$, maximum deviation from the SM prediction is observed with g_{V_L}, g_{V_R}, and g_{T_L} NP couplings and they are clearly distinguishable from the SM prediction. Although the shape of the q^2 distribution is quite similar for g_{V_L} and g_{V_R} couplings, it is, however, quite distinct for g_{T_L} NP coupling.

(iii) In case of $A^\tau_{FB}(q^2)$, we observe a significant deviation from the SM due to g_{V_R}, g_{S_L}, g_{S_R} and g_{T_L} NP couplings. The zero crossing point is shifted to higher values of q^2 than in the SM for g_{V_R}, g_{S_R} and g_{T_L}, whereas, it is shifted to a low value of q^2 for g_{S_L} NP coupling. The observed zero crossings at $q^2 = 6.16 \pm 0.1$ GeV^2, $q^2 = 4.82 \pm 0.2$ GeV^2, $q^2 = 5.54 \pm 0.11$ GeV^2, and $q^2 = 6.49 \pm 0.09$ GeV^2 in the presence of g_{V_R}, g_{S_L}, g_{S_R}, and g_{T_L} are clearly distinguishable from the SM zero crossing of $q^2 = 5.25 \pm 0.10$ GeV^2 at the level of 6.4σ, 2σ, 1.95σ, and 9.21σ significance.

(iv) The observable $A^T_{FB}(q^2)$ shows a significant deviation from SM expectation once g_{V_R} and g_{T_L} NP couplings are switched on. We also observe a zero crossing in $A^T_{FB}(q^2)$ at $q^2 = 5.44 \pm 0.11$ GeV^2 with g_{T_L} NP coupling. Similarly, a significant deviation from the SM prediction is observed in $C^\tau_F(q^2)$ and $F_L(q^2)$ in the presence of g_{T_L} NP coupling. The dip in $C^\tau_F(q^2)$ is shifted to a higher value of q^2 than in the SM.

In Fig. 8, we display q^2 and $\cos\theta_{D_s}$ dependence of several observable for $D_s\gamma$ (left panel) and $D_s\pi$ (right panel) modes. Our main observations are as follows.

(i) In case of DBR(q^2), we observe significant deviation from the SM prediction with g_{T_L}, g_{V_L}, and g_{V_R} NP couplings for both $D_s\gamma$ and $D_s\pi$ modes. The peak of the distribution, however, is shifted to a low value of q^2 than in the SM with g_{T_L} NP coupling.

(ii) The angular observable $A_3(q^2)$ and $A_4(q^2)$ show deviation from the SM in the presence of g_{T_L} NP coupling for both $D_s\gamma$ and $D_s\pi$ modes. Similarly, in case of $A_5(q^2)$, deviation from the SM prediction is observed in the presence of g_{V_R}, g_{S_L}, and g_{T_L} NP coupling in both the decay modes. The deviation in $A_5(q^2)$, however, is more pronounced with g_{T_L} NP coupling.

(iii) Deviation from the SM prediction in $A_{6s}(q^2)$ is observed with g_{S_L}, g_{S_R}, and g_{T_L} NP couplings for the $D_s\gamma$ mode. The deviation is, however, more pronounced in case of g_{T_L} NP coupling. Similarly, for $D_s\pi$ mode, we see significant deviation in $A_{6s}(q^2)$ in the presence of g_{V_R} and g_{T_L} NP couplings. We also observe a zero crossing in the $A_{6s}(q^2)$ at $q^2 = 5.45 \pm 0.11$ GeV^2 with g_{T_L} NP coupling.

(iv) The $A_7(q^2)$ is nonzero with g_{V_R}, g_{S_L}, g_{S_R}, and g_{T_L} NP couplings for both $D_s\gamma$ and $D_s\pi$ decay mode. Similar conclusions can be made for $D_s\pi$ mode as well because of the strict $A_7^\pi = 2A_7^\gamma$ relation.

(v) The angular observables $A_8(q^2)$ and $A_9(q^2)$ are nonzero only in the presence of g_{V_R} NP coupling for both $D_s\gamma$ and $D_s\pi$ modes. We observe a minimum of $A_8(q^2)$ and $A_9(q^2)$ at $q^2 = 7.5$ GeV^2 and $q^2 = 8.28$ GeV^2, respectively.

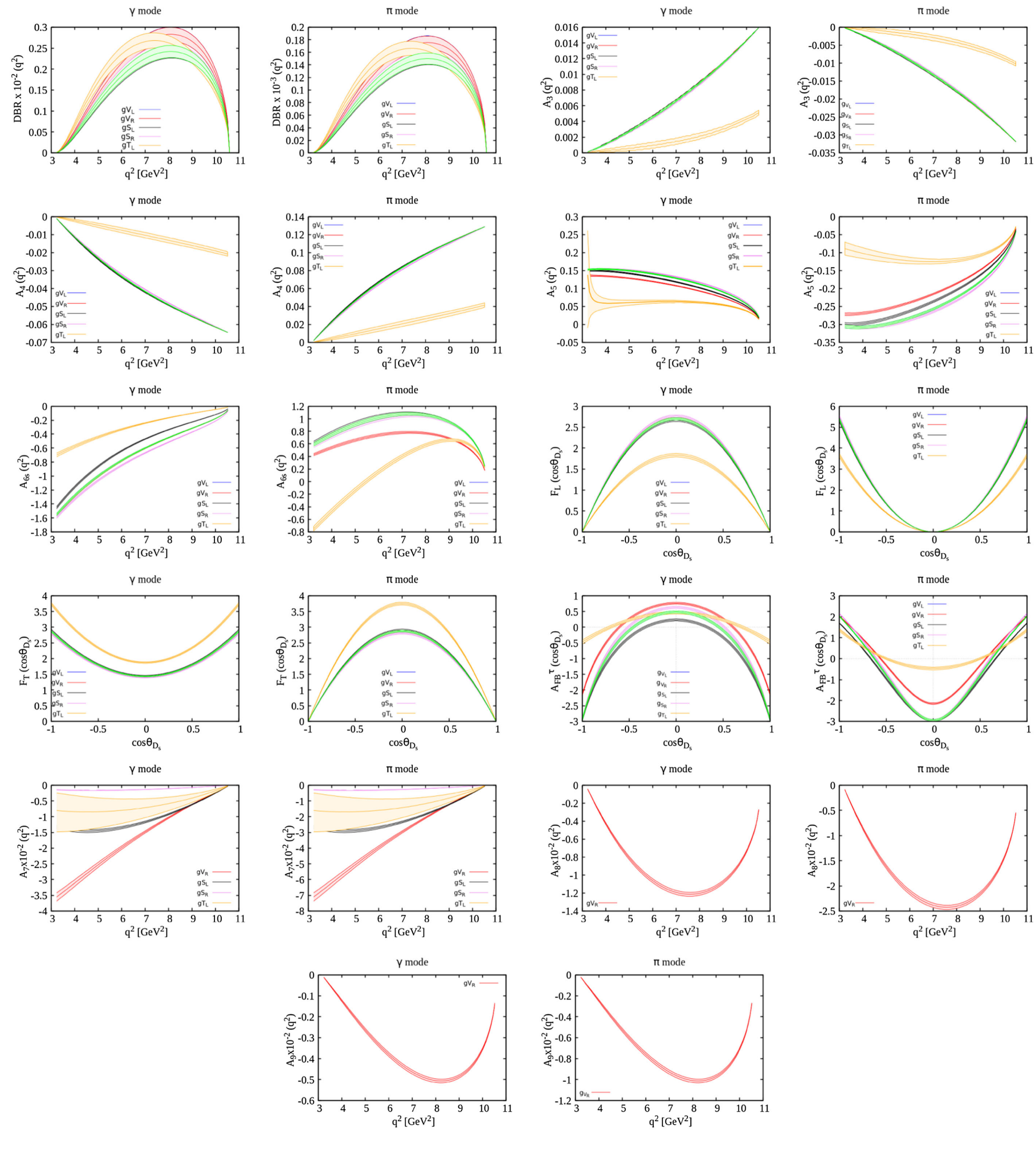

FIG. 8. The q^2 and $\cos\theta_{D_s}$ dependence of various physical observable of $B_s \to D_s^*(\to D_s\gamma, D_s\pi)\tau\nu$ in the SM and in the presence of the NP couplings of scenario III. The SM central line and the corresponding error band are shown with green color. The blue, red, black, violet, and orange colors represents the effect of NP couplings of g_{V_L}, g_{V_R}, g_{S_L}, g_{S_R}, and g_{T_L} respectively.

(vi) Although a slight deviation in $F_L(\cos\theta_{D_s})$ and $F_T(\cos\theta_{D_s})$ is observed with g_{S_R} NP coupling, the deviation, however, is more pronounced with g_{T_L} NP coupling for both $D_s\gamma$ and $D_s\pi$ modes and it is clearly distinguishable from the SM prediction.

(vii) Deviation from the SM prediction in $A_{FB}^{\tau}(\cos\theta_{D_s})$ is observed with g_{V_R} g_{S_L}, g_{S_R}, and g_{T_L} NP couplings for both $D_s\gamma$ and $D_s\pi$ modes. In the $D_s\gamma$ mode, we observe that the zero crossing in $A_{FB}^{\tau}(\cos\theta_{D_s})$ shifts to lower value of $\cos\theta_{D_s}$ than in the SM with g_{V_R},

g_{S_R} and g_{T_L} NP couplings, whereas, it shifts to a higher value of $\cos\theta_{D_s}$ with g_{S_L} NP coupling. The zero crossing points in $A^{\tau}_{FB}(\cos\theta_{D_s})$ at $\cos\theta_{D_s} = \pm 0.605 \pm 0.012, \pm 0.330 \pm 0.025, \pm 0.512 \pm 0.012$ and $\pm 0.703 \pm 0.032$ in the presence of g_{V_R}, g_{S_L}, g_{S_R}, and g_{T_L} NP couplings are clearly distinguishable from the SM zero crossing of $\cos\theta_{D_s} = \pm 0.456 \pm 0.018$ at 6.89σ, 4.09σ, 2.58σ, and 6.72σ significance level, respectively. Similarly, for $D_s\pi$ mode, the zero crossing points in $A_{FB}(\cos\theta_{D_s})$ at $\cos\theta_{D_s} = \pm 0.560 \pm 0.008, \pm 0.663 \pm 0.007, \pm 0.604 \pm 0.0075$ and $\pm 0.500 \pm 0.024$ in the presence of these NP couplings are clearly distinguishable from the SM zero crossing of $\cos\theta_{D_s} = \pm 0.626 \pm 0.007$ at 6σ, 3.6σ, 2.07σ, and 5.01σ level of significance, respectively.

IV. CONCLUSIONS

Motivated by the anomalies present in several $b \to cl\nu$ quark level transition decays, we perform a detail angular analysis of $B_s \to D_s^*(\to D_s\gamma, D_s\pi)l\nu$ decays using the recent lattice QCD form factors. We use the latest global fit results of the possible NP couplings and estimate the effect of each NP couplings on several physical observables pertaining to $D_s\pi$ and $D_s\gamma$ modes in a model independent effective theory formalism.

We first report the SM results. In the SM, we obtain the branching ratio to be of $\mathcal{O}(10^{-2})$ for $D_s\gamma$ channel and $\mathcal{O}(10^{-3})$ for $D_s\pi$ channel. The LHCb collaboration reported the first measurement of the branching ratio to be $\mathcal{B}(B_s^0 \to D_s^{*-}\mu^+\nu_\mu) = (5.38 \pm 0.25 \pm 0.46) \times 10^{-2}$ [106,107] and it is in good agreement with our estimated results for the $D_s\gamma$ mode. The ratio of branching ratio is found to be $R_{D_s^*} = 0.2430 \pm 0.0015$ in the SM.

For our NP analysis we work with three different NP scenarios with the best fit values obtained from various recent global fit results. We assume both real and complex NP couplings in our analysis. We study the underlying observables based on NP contribution coming from single operators ($1D$) as well as from two different operators ($2D$). A brief summary of our results are as follows.

(i) In scenario I, the observable $A^{\tau}_{FB}(q^2)$ is found to be interesting as the zero crossing point observed with g_{S_L} and g_{S_R} and $g_{S_L} = 4g_{T_L}$ NP couplings stand at $1-2\sigma$ away from the SM zero crossing point. Similarly, the effect of g_{V_L} NP coupling is found to be prominent for $\mathrm{DBR}(q^2)$ and $R_{D_s^*}(q^2)$.

(ii) In scenario II, the deviation from the SM prediction observed for $\mathrm{DBR}(q^2)$ and $R_{D_s^*}(q^2)$ is quite significant in the presence of $(g_{V_L}, g_{S_L} = -4g_{T_L})$ and (g_{V_L}, g_{S_R}) NP couplings. The zero crossings in $A^{\tau}_{FB}(q^2)$ with (g_{S_R}, g_{S_L}) and $(g_{S_L} = 4g_{T_L})$ NP couplings are clearly distinguishable from the SM zero crossing point at more than 5σ significance. Similarly, the zero crossing in $A^{\tau}_{FB}(\cos\theta_{D_s})$ obtained with (g_{S_R}, g_{S_L}) and $(g_{S_L} = 4g_{T_L})$ NP couplings are distinguishable from the SM zero crossing at more than 5σ for both the $D_s\gamma$ mode and $D_s\pi$ mode. We find A_7 to be nonzero only in the presence of $g_{S_L} = 4g_{T_L}$ NP coupling.

(iii) In scenario III, the zero crossings in $A^{\tau}_{FB}(q^2)$ in the presence of g_{V_R}, g_{S_L}, g_{S_R}, and g_{T_L} NP couplings are quite different from the SM zero crossing and they are clearly distinguishable from the SM prediction at the level of 6.4σ, 4.8σ, 1.95σ, and 9.21σ significance. We also observe zero crossings in $A^{T}_{FB}(q^2)$ and $A_{6s}(q^2)$ with g_{T_L} NP coupling that are absent in the SM. The angular observable A_7 is found to be nonzero in the presence of g_{V_R}, g_{S_L}, g_{S_R}, and g_{T_L} NP couplings, whereas, A_8 and A_9 are found to be nonzero only for g_{V_R} NP coupling. Moreover, the zero crossing points in $A^{\tau}_{FB}(\cos\theta_{D_s})$ obtained with g_{V_R}, g_{S_L}, g_{S_R}, and g_{T_L} NP couplings are clearly distinguishable from the SM zero crossing at more than 6σ, 4σ, 2σ, and 6σ significance level for the $D_s\gamma$ mode and they are distinguishable at more than 6σ, 3σ, 2σ, and 5σ significance for the $D_s\pi$ mode. In general, the deviation from the SM prediction observed with complex tensor NP coupling g_{T_L} is more pronounced for all the observables in this scenario.

It should be noted that the angular observables $A^{\tau}_{FB}(q^2)$ and $A^{\tau}_{FB}(\cos\theta_{D_s})$ are quite interesting as they can be used to distinguish between several NP scenarios. Similarly, presence of zero crossings in $A^{T}_{FB}(q^2)$ and $A_{6s}(q^2)$ would be a clear signal of complex tensor NP coupling. Moreover, the angular observables A_7, A_8, and A_9 will also play an important role in identifying the exact NP Lorentz structures. In conclusion, the results pertaining to $B_s \to D_s^*(\to D_s\gamma, D_s\pi)l\nu$ decay observables are very useful to explore ongoing flavor anomalies in $b \to cl\nu$ transitions and, in principle, it can provide us complementary information regarding NP in various B meson decays. At the same time, it can also be useful in determining the value of the CKM matrix element $|V_{cb}|$. Moreover, study of these decay modes both theoretically and experimentally can act as a useful ingredient in maximizing future sensitivity to NP.

[1] J. A. Bailey *et al.* (MILC Collaboration), $B \to D\ell\nu$ form factors at nonzero recoil and $|V_{cb}|$ from $2+1$-flavor lattice QCD, Phys. Rev. D **92**, 034506 (2015).

[2] H. Na, C. M. Bouchard, G. P. Lepage, C. Monahan, and J. Shigemitsu (HPQCD Collaboration), $B \to Dl\nu$ form factors at nonzero recoil and extraction of $|V_{cb}|$, Phys. Rev. D **92**, 054510 (2015); **93**, 119906(E) (2016).

[3] S. Aoki *et al.*, Review of lattice results concerning low-energy particle physics, Eur. Phys. J. C **77**, 112 (2017).

[4] D. Bigi and P. Gambino, Revisiting $B \to D\ell\nu$, Phys. Rev. D **94**, 094008 (2016).

[5] F. U. Bernlochner, Z. Ligeti, M. Papucci, and D. J. Robinson, Combined analysis of semileptonic B decays to D and D^*: $R(D^{(*)})$, $|V_{cb}|$, and new physics, Phys. Rev. D **95**, 115008 (2017); **97**, 059902(E) (2018).

[6] S. Jaiswal, S. Nandi, and S. K. Patra, Extraction of $|V_{cb}|$ from $B \to D^{(*)}\ell\nu_\ell$ and the standard model predictions of $R(D^{(*)})$, J. High Energy Phys. 12 (2017) 060.

[7] B. Aubert *et al.* (*BABAR* Collaboration), Measurement of $|V_{cb}|$ and the Form-factor Slope in $\bar{B} \to D\ell^-\bar{\nu}_\ell$ Decays in Events Tagged by a Fully Reconstructed B Meson, Phys. Rev. Lett. **104**, 011802 (2010).

[8] R. Glattauer *et al.* (Belle Collaboration), Measurement of the decay $B \to D\ell\nu_\ell$ in fully reconstructed events and determination of the Cabibbo-Kobayashi-Maskawa matrix element $|V_{cb}|$, Phys. Rev. D **93**, 032006 (2016).

[9] J. P. Lees *et al.* (*BABAR* Collaboration), Evidence for an Excess of $\bar{B} \to D^{(*)}\tau^-\bar{\nu}_\tau$ Decays, Phys. Rev. Lett. **109**, 101802 (2012).

[10] M. Huschle *et al.* (Belle Collaboration), Measurement of the branching ratio of $\bar{B} \to D^{(*)}\tau^-\bar{\nu}_\tau$ relative to $\bar{B} \to D^{(*)}\ell^-\bar{\nu}_\ell$ decays with hadronic tagging at Belle, Phys. Rev. D **92**, 072014 (2015).

[11] A. Abdesselam *et al.* (Belle Collaboration), Measurement of $\mathcal{R}(D)$ and $\mathcal{R}(D^*)$ with a semileptonic tagging method, arXiv:1904.08794.

[12] S. Fajfer, J. F. Kamenik, and I. Nisandzic, On the $B \to D^*\tau\bar{\nu}_\tau$ sensitivity to new physics, Phys. Rev. D **85**, 094025 (2012).

[13] D. Bigi, P. Gambino, and S. Schacht, $R(D^*)$, $|V_{cb}|$, and the heavy quark symmetry relations between form factors, J. High Energy Phys. 11 (2017) 061.

[14] C. Bernard *et al.*, The $\bar{B} \to D^*\ell\bar{\nu}$ form factor at zero recoil from three-flavor lattice QCD: A model independent determination of $|V_{cb}|$, Phys. Rev. D **79**, 014506 (2009).

[15] J. A. Bailey *et al.* (Fermilab Lattice and MILC Collaborations), Update of $|V_{cb}|$ from the $\bar{B} \to D^*\ell\bar{\nu}$ form factor at zero recoil with three-flavor lattice QCD, Phys. Rev. D **89**, 114504 (2014).

[16] A. Bazavov *et al.* (Fermilab Lattice and MILC Collaborations), Semileptonic form factors for $B \to D^*\ell\nu$ at nonzero recoil from $2+1$-flavor lattice QCD, arXiv: 2105.14019.

[17] J. P. Lees *et al.* (*BABAR* Collaboration), Measurement of an excess of $\bar{B} \to D^{(*)}\tau^-\bar{\nu}_\tau$ decays and implications for charged Higgs bosons, Phys. Rev. D **88**, 072012 (2013).

[18] S. Hirose *et al.* (Belle Collaboration), Measurement of the τ Lepton Polarization and $R(D^*)$ in the Decay $\bar{B} \to D^*\tau^-\bar{\nu}_\tau$, Phys. Rev. Lett. **118**, 211801 (2017).

[19] S. Hirose *et al.* (Belle Collaboration), Measurement of the τ lepton polarization and $R(D^*)$ in the decay $\bar{B} \to D^*\tau^-\bar{\nu}_\tau$ with one-prong hadronic τ decays at Belle, Phys. Rev. D **97**, 012004 (2018).

[20] R. Aaij *et al.* (LHCb Collaboration), Measurement of the Ratio of Branching Fractions $\mathcal{B}(\bar{B}^0 \to D^{*+}\tau^-\bar{\nu}_\tau)/\mathcal{B}(\bar{B}^0 \to D^{*+}\mu^-\bar{\nu}_\mu)$, Phys. Rev. Lett. **115**, 111803 (2015); **115**, 159901(E) (2015).

[21] R. Aaij *et al.* (LHCb Collaboration), Test of lepton flavor universality by the measurement of the $B^0 \to D^{*-}\tau^+\nu_\tau$ branching fraction using three-prong τ decays, Phys. Rev. D **97**, 072013 (2018).

[22] A. Abdesselam *et al.* (Belle Collaboration), Measurement of $\mathcal{R}(D)$ and $\mathcal{R}(D^*)$ with a semileptonic tagging method, arXiv:1904.08794.

[23] M. A. Ivanov, J. G. Korner, and P. Santorelli, The semileptonic decays of the B_c meson, Phys. Rev. D **63**, 074010 (2001).

[24] D. Ebert, R. N. Faustov, and V. O. Galkin, Weak decays of the B_c meson to charmonium and D mesons in the relativistic quark model, Phys. Rev. D **68**, 094020 (2003).

[25] A. Abd El-Hady, J. H. Munoz, and J. P. Vary, Semileptonic and nonleptonic B(c) decays, Phys. Rev. D **62**, 014019 (2000).

[26] W. F. Wang, Y. Y. Fan, and Z. J. Xiao, Semileptonic decays $B_c \to (\eta_c, J/\Psi)l\nu$ in the perturbative QCD approach, Chin. Phys. C **37**, 093102 (2013).

[27] Y. K. Hsiao and C. Q. Geng, Branching fractions of $B_{(c)}$ decays involving J/ψ and $X(3872)$, Chin. Phys. C **41**, 013101 (2017).

[28] R. Dutta and A. Bhol, $B_c \to (J/\psi, \eta_c)\tau\nu$ semileptonic decays within the standard model and beyond, Phys. Rev. D **96**, 076001 (2017).

[29] R. Dutta, Exploring R_D, R_{D^*} and $R_{J/\Psi}$ anomalies, arXiv:1710.00351.

[30] T. D. Cohen, H. Lamm, and R. F. Lebed, Model-independent bounds on $R(J/\psi)$, J. High Energy Phys. 09 (2018) 168.

[31] J. Harrison, C. T. H. Davies, and A. Lytle (HPQCD Collaboration), $B_c \to J/\psi$ form factors for the full q^2 range from lattice QCD, Phys. Rev. D **102**, 094518 (2020).

[32] S. Hirose *et al.* (Belle Collaboration), Measurement of the τ Lepton Polarization and $R(D^*)$ in the Decay $\bar{B} \to D^*\tau^-\bar{\nu}_\tau$, Phys. Rev. Lett. **118**, 211801 (2017).

[33] S. Hirose *et al.* (Belle Collaboration), Measurement of the τ lepton polarization and $R(D^*)$ in the decay $\bar{B} \to D^*\tau^-\bar{\nu}_\tau$ with one-prong hadronic τ decays at Belle, Phys. Rev. D **97**, 012004 (2018).

[34] M. Tanaka and R. Watanabe, New physics in the weak interaction of $\bar{B} \to D^{(*)}\tau\bar{\nu}$, Phys. Rev. D **87**, 034028 (2013).

[35] A. Abdesselam *et al.* (Belle Collaboration), Measurement of the D^{*-} polarization in the decay $B^0 \to D^{*-}\tau^+\nu_\tau$, arXiv: 1903.03102.

[36] A. K. Alok, D. Kumar, S. Kumbhakar, and S. U. Sankar, D^* polarization as a probe to discriminate new physics in $\bar{B} \to D^*\tau\bar{\nu}$, Phys. Rev. D **95**, 115038 (2017).

[37] Y. Sakaki, M. Tanaka, A. Tayduganov, and R. Watanabe, Probing new physics with q^2 distributions in $\bar{B} \to D^{(*)}\tau\bar{\nu}$, Phys. Rev. D **91**, 114028 (2015).

[38] P. Biancofiore, P. Colangelo, and F. De Fazio, On the anomalous enhancement observed in $B \to D\tau\bar{\nu}_\tau$ decays, Phys. Rev. D **87**, 074010 (2013).
[39] M. Freytsis, Z. Ligeti, and J. T. Ruderman, Flavor models for $\bar{B} \to D^{(*)}\tau\bar{\nu}$, Phys. Rev. D **92**, 054018 (2015).
[40] R. Dutta, $\Lambda_b \to (\Lambda_c, p)\tau\nu$ decays within standard model and beyond, Phys. Rev. D **93**, 054003 (2016).
[41] S. Bhattacharya, S. Nandi, and S. K. Patra, Looking for possible new physics in $B \to D^{(*)}\tau\nu_\tau$ in light of recent data, Phys. Rev. D **95**, 075012 (2017).
[42] P. Colangelo and F. De Fazio, Tension in the inclusive versus exclusive determinations of $|V_{cb}|$: A possible role of new physics, Phys. Rev. D **95**, 011701 (2017).
[43] R. Dutta and A. Bhol, $b \to (c, , u), \tau\nu$ leptonic and semi-leptonic decays within an effective field theory approach, Phys. Rev. D **96**, 036012 (2017).
[44] A. K. Alok, D. Kumar, J. Kumar, S. Kumbhakar, and S. U. Sankar, New physics solutions for R_D and R_{D^*}, J. High Energy Phys. 09 (2018) 152.
[45] A. Azatov, D. Bardhan, D. Ghosh, F. Sgarlata, and E. Venturini, Anatomy of $b \to c\tau\nu$ anomalies, J. High Energy Phys. 11 (2018) 187.
[46] S. Bifani, S. Descotes-Genon, A. Romero Vidal, and M. H. Schune, Review of lepton universality tests in B decays, J. Phys. G **46**, 023001 (2019).
[47] Z. R. Huang, Y. Li, C. D. Lu, M. A. Paracha, and C. Wang, Footprints of new physics in $b \to c\tau\nu$ transitions, Phys. Rev. D **98**, 095018 (2018).
[48] Q. Y. Hu, X. Q. Li, and Y. D. Yang, $b \to c\tau\nu$ transitions in the standard model effective field theory, Eur. Phys. J. C **79**, 264 (2019).
[49] F. Feruglio, P. Paradisi, and O. Sumensari, Implications of scalar and tensor explanations of $R_{D^{(*)}}$, J. High Energy Phys. 11 (2018) 191.
[50] M. Jung and D. M. Straub, Constraining new physics in $b \to c\ell\nu$ transitions, J. High Energy Phys. 01 (2019) 009.
[51] A. Datta, S. Kamali, S. Meinel, and A. Rashed, Phenomenology of $\Lambda_b \to \Lambda_c\tau\bar{\nu}_\tau$ using lattice QCD calculations, J. High Energy Phys. 08 (2017) 131.
[52] F. U. Bernlochner, Z. Ligeti, D. J. Robinson, and W. L. Sutcliffe, New Predictions for $\Lambda_b \to \Lambda_c$ Semileptonic Decays and Tests of Heavy Quark Symmetry, Phys. Rev. Lett. **121**, 202001 (2018).
[53] A. K. Alok, D. Kumar, S. Kumbhakar, and S. Uma Sankar, Resolution of R_D/R_{D^*} puzzle, Phys. Lett. B **784**, 16 (2018).
[54] R. Dutta, Phenomenology of $\Xi_b \to \Xi_c\tau\nu$ decays, Phys. Rev. D **97**, 073004 (2018).
[55] R. Dutta and N. Rajeev, Signature of lepton flavor universality violation in $B_s \to D_s\tau\nu$ semileptonic decays, Phys. Rev. D **97**, 095045 (2018).
[56] S. Fajfer, J. F. Kamenik, I. Nisandzic, and J. Zupan, Implications of Lepton Flavor Universality Violations in B Decays, Phys. Rev. Lett. **109**, 161801 (2012).
[57] A. Crivellin, C. Greub, and A. Kokulu, Explaining $B \to D\tau\nu$, $B \to D^*\tau\nu$ and $B \to \tau\nu$ in a 2HDM of type III, Phys. Rev. D **86**, 054014 (2012).
[58] X. Q. Li, Y. D. Yang, and X. Zhang, Revisiting the one leptoquark solution to the $R_{D^{(*)}}$ anomalies and its phenomenological implications, J. High Energy Phys. 08 (2016) 054.
[59] B. Bhattacharya, A. Datta, J. P. Guévin, D. London, and R. Watanabe, Simultaneous explanation of the R_K and $R_{D^{(*)}}$ puzzles: A model analysis, J. High Energy Phys. 01 (2017) 015.
[60] D. Leljak and B. Melic, $|V_{ub}|$ determination and testing of lepton flavour universality in semileptonic $B_c \to D^{(*)}$ decays, J. High Energy Phys. 02 (2020) 171.
[61] D. Bečirević, M. Fedele, I. Nišandžić, and A. Tayduganov, Lepton flavor universality tests through angular observables of $\bar{B} \to D^{(*)}\ell\bar{\nu}$ decay modes, arXiv:1907.02257.
[62] N. Rajeev and R. Dutta, Impact of vector new physics couplings on $B_s \to (K, K^*)\tau\nu$ and $B \to \pi\tau\nu$ decays, Phys. Rev. D **98**, 055024 (2018).
[63] R. Dutta, Predictions of $B_c \to (D, D^*)\tau\nu$ decay observables in the standard model, J. Phys. G **46**, 035008 (2019).
[64] P. Colangelo and F. De Fazio, Scrutinizing $\bar{B} \to D^*(D\pi)\ell^-\bar{\nu}_\ell$ and $\bar{B} \to D^*(D\gamma)\ell^-\bar{\nu}_\ell$ in search of new physics footprints, J. High Energy Phys. 06 (2018) 082.
[65] D. Bardhan, P. Byakti, and D. Ghosh, A closer look at the R_D and R_{D^*} anomalies, J. High Energy Phys. 01 (2017) 125.
[66] Y. Li and C. D. Lü, Recent anomalies in B physics, Sci. Bull. **63**, 267 (2018).
[67] J. D. Gómez, N. Quintero, and E. Rojas, Charged current $b \to c\tau\bar{\nu}_\tau$ anomalies in a general W' boson scenario, Phys. Rev. D **100**, 093003 (2019).
[68] A. K. Alok, D. Kumar, S. Kumbhakar, and S. Uma Sankar, New physics solutions for $b \to c\tau\bar{\nu}$ anomalies before and after Moriond 2019, Nucl. Phys. **B953**, 114957 (2020).
[69] N. Rajeev, R. Dutta, and S. Kumbhakar, Implication of $R_{D^{(*)}}$ anomalies on semileptonic decays of Σ_b and Ω_b baryons, Phys. Rev. D **100**, 035015 (2019).
[70] H. Yan, Y. D. Yang, and X. B. Yuan, Phenomenology of $b \to c\tau\bar{\nu}$ decays in a scalar leptoquark model, Chin. Phys. C **43**, 083105 (2019).
[71] O. Popov, M. A. Schmidt, and G. White, R_2 as a single leptoquark solution to $R_{D^{(*)}}$ and $R_{K^{(*)}}$, Phys. Rev. D **100**, 035028 (2019).
[72] K. Azizi, Y. Sarac, and H. Sundu, Lepton flavor universality violation in semileptonic tree level weak transitions, Phys. Rev. D **99**, 113004 (2019).
[73] X. L. Mu, Y. Li, Z. T. Zou, and B. Zhu, Investigation of effects of new physics in $\Lambda_b \to \Lambda_c\tau\bar{\nu}_\tau$ decay, Phys. Rev. D **100**, 113004 (2019).
[74] K. Azizi, A. T. Olgun, and Z. Tavukoglu, Effects of vector leptoquarks on $\Lambda_b \to \Lambda_c\ell\bar{\nu}_\ell$ decay, Chin. Phys. C **45**, 013113 (2021).
[75] P. Colangelo, F. De Fazio, and F. Loparco, Probing new physics with $\bar{B} \to \rho(770)\ell^-\bar{\nu}_\ell$ and $\bar{B} \to a_1(1260)\ell^-\bar{\nu}_\ell$, Phys. Rev. D **100**, 075037 (2019).
[76] W. Altmannshofer, P. S. Bhupal Dev, and A. Soni, $R_{D^{(*)}}$ anomaly: A possible hint for natural supersymmetry with R-parity violation, Phys. Rev. D **96**, 095010 (2017).
[77] Z. Rui, H. Li, G. x. Wang, and Y. Xiao, Semileptonic decays of B_c meson to S-wave charmonium states in the perturbative QCD approach, Eur. Phys. J. C **76**, 564 (2016).

[78] B. Bhattacharya, A. Datta, S. Kamali, and D. London, CP Violation in $\bar{B}^0 \to D^{*+}\mu^-\bar{\nu}_\mu$, J. High Energy Phys. 05 (2019) 191.
[79] R. X. Shi, L. S. Geng, B. Grinstein, S. Jäger, and J. Martin Camalich, Revisiting the new-physics interpretation of the $b \to c\tau\nu$ data, J. High Energy Phys. 12 (2019) 065.
[80] B. Bhattacharya, A. Datta, S. Kamali, and D. London, A measurable angular distribution for $\bar{B} \to D^*\tau^-\bar{\nu}_\tau$ decays, J. High Energy Phys. 07 (2020) 194.
[81] L. Zhang, X. W. Kang, X. H. Guo, L. Y. Dai, T. Luo, and C. Wang, A comprehensive study on the semileptonic decay of heavy flavor mesons, J. High Energy Phys. 02 (2021) 179.
[82] M. Blanke, A. Crivellin, S. de Boer, T. Kitahara, M. Moscati, U. Nierste, and I. Nišandžić, Impact of polarization observables and $B_c \to \tau\nu$ on new physics explanations of the $b \to c\tau\nu$ anomaly, Phys. Rev. D **99**, 075006 (2019).
[83] M. Blanke, A. Crivellin, T. Kitahara, M. Moscati, U. Nierste, and I. Nišandžić, Addendum to pact of polarization observables and $B_c \to \tau\nu$ on new physics explanations of the $b \to c\tau\nu$ anomaly, Phys. Rev. D **100**, 035035 (2019).
[84] C. Murgui, A. Peñuelas, M. Jung, and A. Pich, Global fit to $b \to c\tau\nu$ transitions, J. High Energy Phys. 09 (2019) 103.
[85] S. M. Zhao, X. Liu, and S. J. Li, Study on $B_s \to D_{(\mathrm{sJ})}$ (2317, 2460) $l\nu$ semileptonic decays in the CQM model, Eur. Phys. J. C **51**, 601 (2007).
[86] K. Azizi and M. Bayar, Semileptonic $B(q) \to D_q^* l\nu$ $(q = s, d, u)$ decays in QCD sum rules, Phys. Rev. D **78**, 054011 (2008).
[87] M. Bayar and K. Azizi, Semileptonic $B(q) \to D_q^* l\nu$ $(q = s,\ d,\ u)$ transitions in QCD, Nucl. Phys. B, Proc. Suppl. **186**, 395 (2009).
[88] R. H. Li, C. D. Lu, and Y. M. Wang, Exclusive B(s) decays to the charmed mesons $D(s) + (1968, 2317)$ in the standard model, Phys. Rev. D **80**, 014005 (2009).
[89] M. Bordone, N. Gubernari, D. van Dyk, and M. Jung, Heavy-quark expansion for $\bar{B}_s \to D_s^{(*)}$ form factors and unitarity bounds beyond the $SU(3)_F$ limit, Eur. Phys. J. C **80**, 347 (2020).
[90] G. Li, F. l. Shao, and W. Wang, $B_s \to D_s(3040)$ form factors and B_s decays into $D_s(3040)$, Phys. Rev. D **82**, 094031 (2010).
[91] X. J. Chen, H. F. Fu, C. S. Kim, and G. L. Wang, Estimating form factors of $B_s \to D_s^{(*)}$ and their applications to semi-leptonic and non-leptonic decays, J. Phys. G **39**, 045002 (2012).
[92] T. Zhou, T. h. Wang, Y. Jiang, X. Z. Tan, G. Li, and G. L. Wang, Relativistic calculations of $R(D^{(*)})$, $R(D_s^{(*)})$, $R(\eta_c)$ and $R(J/\psi)$, Int. J. Mod. Phys. A **35**, 2050076 (2020).
[93] J. Harrison, C. T. H. Davies, and M. Wingate (HPQCD Collaboration), Lattice QCD calculation of the $B_{(s)} \to D_{(s)}^* \ell\nu$ form factors at zero recoil and implications for $|V_{cb}|$, Phys. Rev. D **97**, 054502 (2018).
[94] Y. Y. Fan, W. F. Wang, and Z. J. Xiao, Study of $\bar{B}_s^0 \to (D_s^+, D_s^{*+})l^-\bar{\nu}_l$ decays in the pQCD factorization approach, Phys. Rev. D **89**, 014030 (2014).
[95] S. Sahoo and R. Mohanta, Investigating the role of new physics in $b \to c\tau\bar{\nu}_\tau$ transitions, arXiv:1910.09269.
[96] T. D. Cohen, H. Lamm, and R. F. Lebed, Precision model-independent bounds from global analysis of $b \to c\ell\nu$ form factors, Phys. Rev. D **100**, 094503 (2019).
[97] R. N. Faustov and V. O. Galkin, Weak decays of B_s mesons to D_s mesons in the relativistic quark model, Phys. Rev. D **87**, 034033 (2013).
[98] N. Das and R. Dutta, Implication of $b \to c\tau\nu$ flavor anomalies on $B_s \to D_s^*\tau\nu$ decay observables, J. Phys. G **47**, 115001 (2020).
[99] B. Pal *et al.* (Belle Collaboration), Observation of the Decay $B_s^0 \to K^0\bar{K}^0$, Phys. Rev. Lett. **116**, 161801 (2016).
[100] J. Harrison *et al.* (LATTICE-HPQCD Collaboration), $B_s \to D_s^*$ form factors for the full q^2 range from lattice QCD, arXiv:2105.11433.
[101] T. Bhattacharya, V. Cirigliano, S. D. Cohen, A. Filipuzzi, M. Gonzalez-Alonso, M. L. Graesser, R. Gupta, and H. W. Lin, Probing novel scalar and tensor interactions from (Ultra)Cold neutrons to the LHC, Phys. Rev. D **85**, 054512 (2012).
[102] V. Cirigliano, J. Jenkins, and M. Gonzalez-Alonso, Semileptonic decays of light quarks beyond the standard model, Nucl. Phys. **B830**, 95 (2010).
[103] P. Colangelo, F. De Fazio, and F. Loparco, Role of $B_c^+ \to B_{s,d}^{(*)}\bar{\ell}\nu_\ell$ in the Standard Model and in the search for BSM signals, Phys. Rev. D **103**, 075019 (2021).
[104] R. Mandal, C. Murgui, A. Peñuelas, and A. Pich, The role of right-handed neutrinos in $b \to c\tau\bar{\nu}$ anomalies, J. High Energy Phys. 08 (2020) 022.
[105] P. A. Zyla *et al.* (Particle Data Group), Review of particle physics, Prog. Theor. Exp. Phys. **2020**, 083C01 (2020).
[106] R. Aaij *et al.* (LHCb Collaboration), Measurement of $|V_{cb}|$ with $B_s^0 \to D_s^{(*)-}\mu^+\nu_\mu$ decays, Phys. Rev. D **101**, 072004 (2020).
[107] R. Aaij *et al.* (LHCb Collaboration), Measurement of the shape of the $B_s^0 \to D_s^{*-}\mu^+\nu_\mu$ differential decay rate, J. High Energy Phys. 12 (2020) 144.